Knee Joint Contact Forces during Cycling

Estimating medial and lateral condylar force distribution using musculoskeletal modelling and experimental data

J.M. van den Broek

Delft University of Technology

TU Delft

Knee Joint Contact Forces during Cycling

Estimating medial and lateral condylar force distribution using musculoskeletal modelling and experimental data

by

J.M. van den Broek

To obtain the degree of Master of Science
Mechanical Engineering, BioMechanical Design, at the Delft University of Technology,
to be defended publicly on Friday June 13, 2025 at 11:45 AM.

Student Number:	4683676
Project Duration:	September 1, 2024 - June 13, 2025
Thesis Committee:	Prof. Dr. Ir. Jaap Harlaar
	Dr. Wouter Schallig
	Dr. Ir. Ajay Seth
	Sabrina Hörmann MSc
	Dr. J. Micah Prendergast
Faculty:	Faculty of Mechanical Engineering, Delft
Department:	Department of Biomechanical Engineering (BMech)
Course Code:	ME51035

TU Delft

Preface

This thesis marks the end of my time as a student. Over the past eight years of studying Mechanical Engineering, I have always valued the broad range of engineering principles the field covers. For my graduation project, I was privileged to apply those principles in a clinical setting, helping develop the MOBI laboratory at Erasmus Medical Center. In many ways, this project brought that wide range of engineering into full effect. I found myself working across multiple research groups, guiding participants, diving into the fine details of musculoskeletal models, while also drilling, assembling, and arranging the equipment needed to get the lab operational. It was sometimes challenging, but just as often rewarding.

I would like to thank my chair, Jaap, for his endless enthusiasm about using technology to advance the lab and its research (i.e. soldering lessons and discussions about electrical circuits on the lab floor). Thanks also to Ajay, for welcoming me into his CBL group and supporting me with my musculoskeletal models, as well as for the insightful and often enjoyable discussions about my methods and interpretation. A special thanks to Wouter, who was involved in every part of this project: from shaping the idea, to the development of the model and the execution of the experiments. Your flexibility when plans changed, and our ability to shift the topic to football or anything else when needed, was something I truly appreciated. I also would like to thank Sabrina, who became almost an extra daily supervisor. I could ask every possible question on my model or the results possible, and you were always there with guidance, even when there was no clear answer. The response time from both you and Wouter throughout this project was truly exceptional. I would like to thank Micah Prendergast for being part of my thesis graduation committee.

I want to express my appreciation for the other students and researchers of both the 'Clinical Biomechanics' and 'Computational Biomechanics Lab'. Your questions, answers, discussions, and feedback helped me a lot during the project. I really hope these groups will continue on working on the interesting research they are conducting, and that more students after me will have the chance to be part of both groups. A big thanks to the eleven participants who took part in my experiments and hopped on the bike for science. I would also like to extend my gratitude to Pijke and Gijs (the model) for designing the report cover. Last but not least, I would like to thank my family, friends, roommates, and Lucie, for helping me put things in perspective, supporting me throughout the project, and being there when it was time to take a break.

Thank you for taking the time to read this thesis. I truly appreciate your interest and effort. It has been a rewarding process full of learning and discovery for me, and I hope that, in reading it, you find some of that same curiosity and interest.

J.M. van den Broek
Rotterdam, June 2025

Abstract

Introduction: Knee osteoarthritis (KOA) is a degenerative joint condition that affects both the medial and lateral femoral condyles, and is a leading cause of pain and reduced mobility worldwide. Low-impact exercises such as cycling are increasingly explored, as cycling reduces knee joint contact forces (KJCF) compared to high-impact activities, making it a suitable option for preserving joint health. Understanding the distribution of KJCF across the medial and lateral condyles during cycling is crucial for informing effective exercise interventions.

Objective: This study aims to validate an existing musculoskeletal cycling model using experimental electromyography (EMG) data, and to extend it to estimate the distribution of the tibiofemoral compressive force (TFC) across the medial and lateral condyles.

Methods: Eleven healthy recreational cyclists (mean age: 25.7 ± 1.7 years) participated in lab-based cycling trials. Reflective markers and EMG sensors captured lower limb kinematics and muscle activity at varying cadences (70–90 RPM) and power outputs (80–120 W).
The musculoskeletal cycling model of Clancy et al. (2023) in OpenSim was modified to include separate medial and lateral knee compartments. A publicly available dataset was used to scale the modified model and run inverse kinematics (IK), static optimisation (SO), and joint reaction force (JRF) analysis. Predicted muscle activation was evaluated using five matched comparison pairs and cross-correlation analysis. Finally, the modified model was used to estimate the distribution of TFC across the medial and lateral condyles throughout the crank cycle.

Results: The modified model produced near-identical results compared to the original model in both muscle activation ($R > 0.99$) and total TFC ($R > 0.98$), verifying the model modifications. Model-predicted muscle activations showed the highest correlation with EMG data for the vastus medialis (VM) ($R = 0.88$–0.99) and the vastus lateralis (VL) ($R = 0.84$–0.99). Lower correlations were observed for the rectus femoris (RF), gastrocnemii (GL, GM), biceps femoris (BF), and semitendinosus (ST). In all subjects, lateral TFC consistently exceeded medial TFC throughout most of the crank cycle.

Conclusion: This thesis successfully estimated compartmental TFC during cycling without affecting the muscle activations or total TFC predictions. Comparison with EMG data showed variable agreement, reflecting modelling limitations and inter-subject variability. The results provide valuable insight into asymmetrical knee joint loading during cycling and illustrate the potential of musculoskeletal modelling to guide more targeted rehabilitation strategies for individuals with KOA.

Contents

1

Introduction

Osteoarthritis (OA) is a degenerative joint condition that causes pain, swelling, and stiffness, leading to reduced mobility of the joint [1]. It is the most common form of arthritis, affecting more than 7% of the global population [2]. The knee joint is among the most frequently affected joints [2, 3]. Knee Osteoarthritis (KOA) usually develops in middle age and is a prevalent cause of disability, contributing to a decline in overall quality of life [4]. Globally, approximately 650 million people over the age of 40 are suffering from KOA [5], and this number is projected to increase by 75% by 2050 [2]. As KOA continues to affect a growing number of individuals, the associated burden on healthcare systems is expected to grow correspondingly [6], underscoring the need for effective symptom management strategies to help maintain patients' quality of life.

The progression of KOA is strongly influenced by joint loading, which accelerates cartilage wear and degeneration [5, 7]. Knee cartilage is thought to adapt to repetitive loading patterns of activities such as walking, maintaining its structure through balanced mechanical and biological responses [8]. However, disruptions in regular loading patterns due to injury, altered gait, or excessive load can subject cartilage to stress in regions not conditioned to bear it, triggering degeneration and contributing to KOA progression [8]. A key factor influencing these abnormal loading patterns is body mass. Individuals with higher body mass indices (BMI), such as those who are overweight or obese, face greater mechanical loads on the knee, increasing their risk of KOA. Within the knee joint, both the medial and lateral condyles can be affected [9], however, the medial compartment is most commonly involved. This vulnerability has been attributed to the higher mechanical loads placed on the medial side during standard movement patterns such as walking [10]. As a result, the medial compartment has become a primary focus of biomechanical and clinical research [11, 12].

An improved understanding of compartment-specific mechanical load disctribution is not only relevant for research but also critical for informing treatment strategies, especially in the absence of a cure for KOA. While surgical interventions such as knee replacements remain a common option, they are costly, invasive, and associated with substantial risks, including reduced range of motion (ROM), post-operative stiffness, and joint pain [13, 14]. Therefore, delaying surgery and prioritizing non-invasive treatment strategies is essential [15].

In this context, the Osteoarthritis Research Society International (OARSI) recommends exercise therapy as a primary treatment for KOA due to its proven effectiveness and non-invasive nature [16]. Managing KOA through exercise therapy helps stabilize the knee by strengthening the surrounding muscles [17]. However, not all types of physical activity are suitable. High impact joint exercises, such as soccer, tennis, and long-distance running, can increase joint loading and pain, as well as the risk of developing or worsening KOA [11, 18]. In other words: exercise is beneficial, but too much weight-bearing activity can be detrimental. This highlights the need for low-impact exercises that provide the benefits of movement without placing too high loads on the knee.

Cycling is such an activity, offering joint loading that is safer for the knee compared to high-impact exercises, and an effective way to stay active [19, 20, 21]. Research has demonstrated that cycling reduces knee pain and disability among KOA patients, and helps improve impairments such as decreased ROM and muscle strength [4, 19, 22]. These benefits make cycling advantageous for knee health and KOA

patients [21, 23].

Furthermore, research indicates that lifelong recreational cycling can reduce the risk of symptomatic KOA by nearly 50% [24], emphasizing its potential as a non-pharmacological intervention for KOA management. In the Netherlands, cycling is widely practiced and commonly incorporated into rehabilitation programs to strengthen the knees and help individuals maintain a higher quality of life over longer periods [25, 26].

1.1. Knee joint contact forces

While clinical studies have demonstrated the benefits of cycling for individuals with KOA, the biomechanical mechanisms underlying these benefits remain poorly understood [27]. In particular, the distribution of knee joint contact forces (KJCF) during cycling remains largely unknown [28], especially regarding the compressive forces across the medial and lateral condyles. Given that KOA can affect either the medial or lateral condyle, understanding how KJCF are distributed across these condyles during a low-impact activity like cycling may help clarify the role of cycling in mitigating condyle-specific KOA progression.

To better understand the distribution of KJCF during cycling, it is first important to consider the anatomical structure of the knee and the types of KJCF involved.

The knee is a complex weight-bearing joint [29], subjected to dynamic loads due to multidirectional forces during cycling [30]. Structurally, the knee joint consists of two primary articulations: the patellofemoral joint (between the patella and femur) and the tibiofemoral joint (between the tibia and femur) [31, 32]. Both joints experience compressive and shear KJCF during cycling. Analyzing these forces is crucial because of their role in weight bearing, joint stability, injury mechanisms, and the progression of KOA [33]. KJCF can be categorized into patellofemoral compressive force (PFC), tibiofemoral compressive force (TFC), and tibiofemoral shear force (TFS) (Figure 1.1). TFS can be directed in both the anterior/posterior and medial/lateral directions. While patellofemoral shear forces (PFS) are present during cycling, they are generally of lower magnitude and are considered to have limited clinical relevance [34].

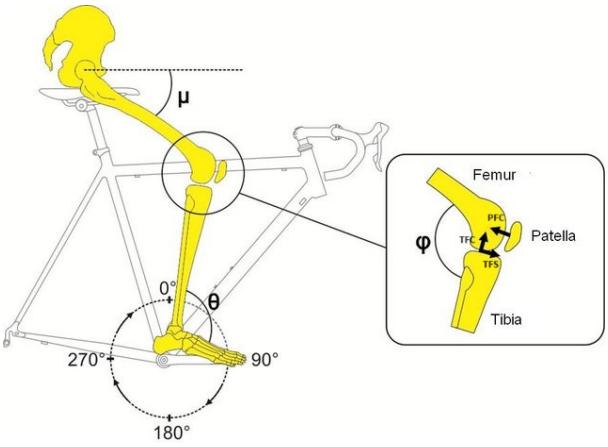

Figure 1.1: Schematic representation of lower limb motion during cycling and the associated knee joint contact forces (KJCF) The figure illustrates the patellofemoral compressive force (PFC), tibiofemoral compressive force (TFC), and tibiofemoral shear force (TFS) acting in this figure in the anterior–posterior direction at the knee joint, adapted from Bini et al. [35].

The magnitude and distribution of KJCF vary depending on the type of activity. For example, high-impact activities such as tennis can generate peak TFC up to four times body weight [36], whereas cycling typically produces peak TFC between 0.3 and 2 times body weight [30, 36, 37].

Despite the relevance of the PFC, TFC, and TFS, most existing cycling studies focus primarily on the total components of these forces. In particular, TFC and TFS are not distinguished between the medial and lateral condyles [22, 34, 38, 39, 40, 41, 42, 43, 44, 45, 46, 47]. In addition, most of these studies focus on performance optimisation in professional or recreational athletes rather than on mechanical loading patterns relevant to clinical populations [41, 43, 45, 46, 48]. Consequently, it remains unclear whether cycling imposes asymmetric loads on the medial and lateral condyles, limiting our ability to assess its relevance for KOA management.

1.2. Musculoskeletal modelling

Direct insights into KJCF are obtained through in-vivo measurements using instrumented joint implants, for example during gait analysis [49, 50, 51, 52]. To our knowledge, only one study has reported in-vivo KJCF during cycling [22]. Because direct measurements are generally not feasible, especially in healthy individuals or large-scale studies, musculoskeletal modelling has become a powerful non-invasive alternative for estimating KJCF [53]. By integrating external forces with muscular activity, these models enhance rigid body kinematics in biomechanical research and allow for simulating KJCF with improved physiological relevance [28, 54]. This has also led to increasing interest in musculoskeletal models that distinguish between medial and lateral KJCF.

Based on a model of Rajagopal et al. [55], several studies have sought to investigate the KJCF in the medial and lateral tibiofemoral condyles during walking. Lerner et al. were the first to incorporate separate medial and lateral knee compartments into a musculoskeletal model, analyzing KJCF distribution during gait [56]. In their model, they introduced frontal plane alignment bodies to represent individual differences in varus and valgus knee alignment. Additionally, they modified the knee joint of Delp et al. [57] and divided it into two parallel condyles. This work laid the foundation for later studies that improved medial-lateral load estimations, by enabling larger knee and hip flexion ranges [58, 59] and by incorporating more realistic muscle tendon properties [60, 61].

Despite these advancements, they have only been applied to gait analysis rather than cycling. Several musculoskeletal models have been used to study KJCF during cycling, such as the one from Clancy et al. [47]. Their model estimated the TFC of 16 participants using kinematic and kinetic data from previous studies [62, 63]. However, it did not explicitly model the medial and lateral compartments separately, and validation of the estimated muscle activity was not possible due to the lack of recorded electromyography (EMG) data.

Accurate estimation of internal forces requires careful modelling of muscle activity, as muscle forces significantly influence KJCF during movement [64]. In cycling specifically, co-contraction of muscles around the knee has been observed [65], further increasing KJCF. Furthermore, increased muscle co-contraction has been observed in individuals with KOA and is thought to be both a consequence of joint degeneration and a potential contributor to its progression [64, 66]. This highlights the importance of accurately estimating muscle activation patterns when studying joint loading and OA-related biomechanics. To accurately estimate these internal forces, musculoskeletal models are used to simulate muscle activity and joint mechanics. Validating model-predicted muscle activations against EMG data is essential for accurately estimating internal joint loading during cycling [67].

Given the compartment-specific nature of KOA, accurate biomechanical modelling of medial and lateral condyle loading is critical. To evaluate the effects of cycling on individuals with compartmental KOA, musculoskeletal models must estimate condyle-specific KJCF rather than total KJCF alone. Without this structural distinction, simulated KJCF fails to capture potentially important differences in load distribution across the knee joint.

This study therefore has two primary objectives. First, it aims to validate the previously discussed musculoskeletal cycling model developed by Clancy et al. through comparison with experimental EMG data. Second, it aims to enhance this model by incorporating medial-lateral condyle separation and estimate the distribution of KJCF during cycling. Together, these developments will provide a more realistic and clinically relevant understanding of force distribution across the knee joint during cycling.

To address these objectives, this study aims to answer the following research questions:

RQ1. *How accurately does the musculoskeletal cycling model by Clancy et al. predict muscle activations, when validated against EMG data from comparable subjects?*

RQ2. *How are total tibiofemoral compressive forces (TFC) distributed across the medial and lateral compartments during cycling, as estimated using a compartment-specific musculoskeletal model?*

2

Methodology

To address the research objectives, a cycling laboratory environment was developed to enable the collection of controlled experimental data. Marker trajectories and surface EMG signals were recorded during cycling trials and used to validate the original musculoskeletal model by Clancy et al. (research question 1). Following validation, the model was enhanced to include separate medial and lateral knee compartments. Muscle activations and total TFC predicted by the modified model were compared to the outputs of the original model, to verify the modifications. These enhancements enabled the estimation of KJCF separately at the medial and lateral condyles (research question 2) (Figure 2.1).

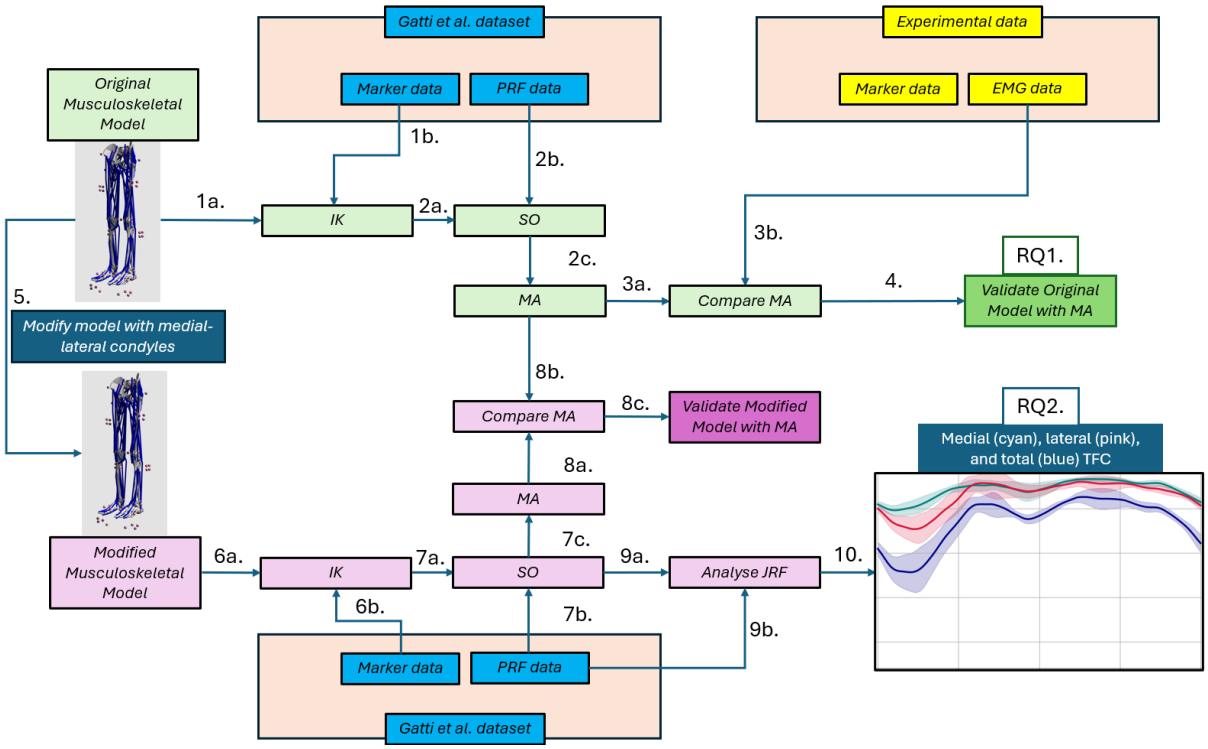

Figure 2.1: Flow chart of the methodology. 1a. Inverse kinematics (IK) with the original model (of Clancy et al. [47]) and marker trajectory data (1b.) from the online dataset. 2a. Static optimisation (SO) with pedal reaction force (PRF) data (2b.) from the online dataset. 2c. Retrieved muscle activations (MA). 3a. Compared MA of the online dataset with electromyography (EMG) data (3b.) from experimental data for similar subjects. 4. Validated the original model (research question 1 (RQ1). 5. Updated original model with medial and lateral compartments and created the modified model. 6a. Ran IK with modified model but with the same marker trajectory data (6b.) as in 1b. 7a. SO with PRF (7b.). 7c. Retrieved MA. 8a. Resulting MA compared with MA from the original model (8b.) to be able to verify the modifications (8c.). 9a. Combined IK, MA and PRF (9b.) in OpenSim's joint reaction force (JRF) analyse tool to compute the knee joint contact forces (KJCF). 10. Plotted mean and standard deviation of the total, medial, and lateral tibiofemoral compressive force (TFC) during a crank cycle (RQ2).

2.1. Experiment protocol

2.1.1. Participants

Eleven participants (age: 25.7 $\pm$ 1.7 years, mass: 76.4 $\pm$ 12.6 kg, height: 182.6 $\pm$ 8.4 cm) were recruited for the experiments. All participants were recreational cyclists, and cycled at least 1.5 hours per week. This study exclusively included healthy individuals, and excluded participants who self-reported knee pain or lower-extremity injuries during the past month. Detailed anthropometric data for each participant are provided in Appendix C. Each participant gave their informed consent to participate in this study. The experimental protocol was approved by the Human Research Ethics Committee (HREC) of the Technical University of Delft. The experimental protocol can be found in Appendix E. The experiments were conducted in the Motion Biomechanics and Imaging (MOBI) lab in the Erasmus Medical Center in Rotterdam.

2.1.2. Optical motion capture

To follow the cycling kinematics of each participant, reflective markers were placed on the lower extremities using the Conventional Gait Model 2.4 (CGM) markerset [68, 69] (Appendix A). Two markers were placed on the crank and one on the extension of the pedal, to define the foot-pedal interaction, and to retrieve the position of the pedal in space (Figure 2.2). The marker trajectories were recorded by 12 infrared cameras (VICON Vero, Oxford, United-Kingdom) and analysed using Nexus Software (v15.9). A detailed description of the development of the MOBI lab can be found in Appendix D.

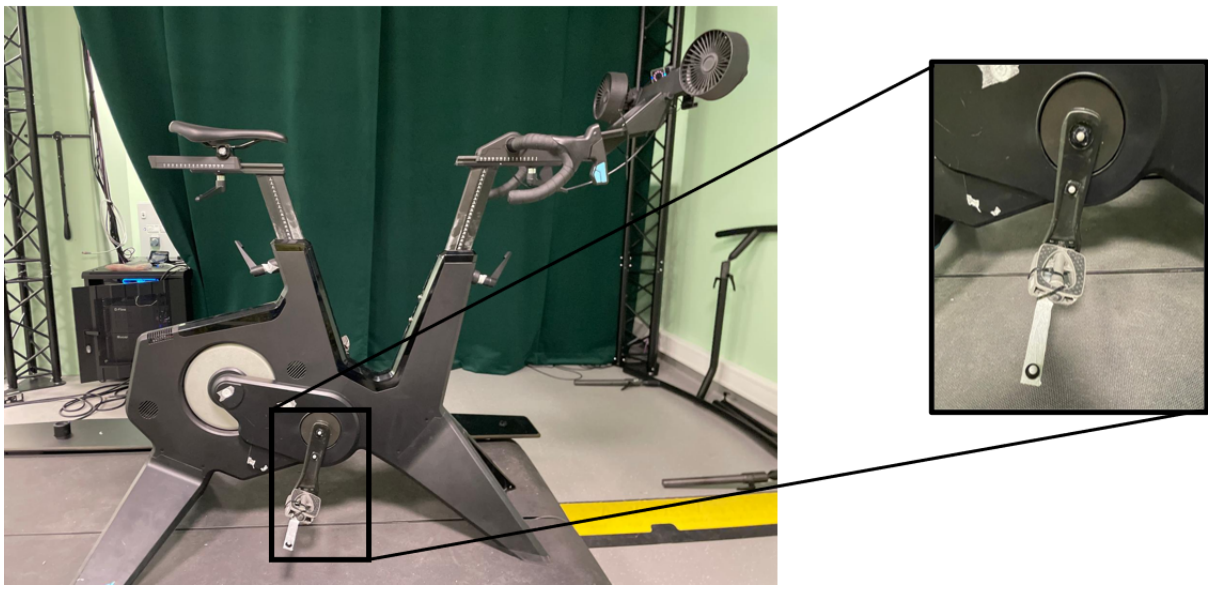

Figure 2.2: Tacx Neo bike in the MOBI lab environment. Reflective pedal markers on the crank axis, the crank arm, and a rigid plate connected to the pedal.

2.1.3. Bike setup

A Neo Tacx bike was used, with a crank arm length of 172.5 mm, which is considered standard [70]. For vertical saddle positioning, a method by Holmes et al. was used [71]. The knee angle was measured when the pedal was at Bottom Dead Centre (BDC), to ensure proper configuration of the saddle height. According to this method, the knee must be flexed between 25° and 30°, which has been related to reduced knee joint load [72] and improved energy efficiency in cycling [73].

The horizontal handlebar position was adjusted to create an approximate 70-90° angle between the torso and upper arms. Participants were then encouraged to provide feedback to fine-tune the handlebar position to their preference [63].

The horizontal saddle position was based on recommendations from the Tacx Neo bike general guidelines [74]. When the right pedal was at Top Dead Centre (TDC), the patella of the right knee should be directly above the centre of the right pedal (Table 2.1).

No instrumented pedals were used in this study to measure the pedal reaction forces (PRF). Although an attempt was made to estimate the PRF after the experiments (Appendix H), they were ultimately

excluded from the scope of this study.

Bike Parameter	Set Value
Crank arm length	172.5 mm
Vertical saddle position	Knee flexion angle between 25° and 30°
Horizontal saddle position	Patella should be directly above the centre of the pedal when the pedal is at BDC
Vertical handlebar position	The handlebar is set at the same height as the saddle
Horizontal handlebar position	70-90° angle between the torso and upper arms

Table 2.1: Bike fitting parameters with their set values.

2.1.4. EMG

EMG-sensors of Cometa [75] were used, which were placed on the participant using the 'Surface Electromyography for the Non-Invasive Assessment of Muscles' (SENIAM) guidelines [76]. These placement recommendations include guidelines for 30 muscles, ensuring consistent and reliable EMG recordings. Sensors were placed on seven muscles of the right leg: Rectus femoris (RF), vastus lateralis (VL), vastus medialis (VM), gastrocnemius lateralis (GL), gastrocnemius medialis (GM), biceps femoris (BF), and semitendinosus (ST) (Appendix E). These muscles were selected based on their major impact on KJCF during cycling [77, 78]. Since we are only interested in the KJCF of the right leg, the muscle activations of the left leg were not measured.

2.1.5. Experimental protocol

Participants performed a brief 2-minute warm-up at a self-chosen cadence and power output to familiarize themselves with the setup. The main cycling session involved nine 30 seconds intervals, each at varying cadences between 70 and 90 RPM and power levels between 80 and 120 watts (Table 2.2), designed to simulate a range of typical cycling intensities without causing fatigue [22]. With the Tacx Training app, the power output was set, and the bike automatically adjusted the gears and resistance to match this set power output at each cadence. The participant only had to keep their cadence constant during the interval. Cadence and the power output were saved in the Garmin Connect app [79]. After each interval there was enough time to change the cadence. Finally, the participants performed a maximum sprint at 200 watts. This maximum sprint will later be used as the participant's maximum voluntary contraction, to normalize the EMG data [60].

Table 2.2: Experimental Cycling Conditions

Phase	Cadence (RPM)	Power Output (W)
Warm-up (2 min)	Self-chosen	Self-chosen
Set 1 (30 sec each)	70	80
	80	80
	90	80
Rest (30 sec)	-	-
Set 2 (30 sec each)	70	100
	80	100
	90	100
Rest (30 sec)	-	-
Set 3 (30 sec each)	70	120
	80	120
	90	120
Rest (10 sec)	-	-
Max Sprint Trial (5 sec)	Self-chosen	200
Cool-down	Self-chosen	Self-chosen

2.2. Datasets

For this study, two types of dataset were used:

1. The online dataset used by Clancy et al. [47].
2. The experimental dataset collected from the cycling experiments (Chapter 2.1).

The online dataset is collected in a study by Gatti et al. [62, 63]. The bike fit in this study by Gatti et al. used a crank arm length of 172.5 mm and set the saddle height at 109% of the inseam length [63]. The same method was used to determine handlebar position, and they also used flat pedals, although they secured the feet with Velcron straps. PRF were collected at 450 Hz using pedals that measure three Degree of Freedom (DOF) forces and moments (Science To Practice, Ljubljana, Slovenia).

All participants cycled at their preferred cadence and at a power output that kept their heart rate (HR) within 70-75% of their age-predicted maximum. Kinematic data were recorded using 12 infrared cameras (Raptor-4, Motion Analysis Corporation, Santa Rosa, CA, USA), and the participants in this online dataset were equipped with 40 reflective markers.

2.3. Data analysis

The motion capture and EMG data were time-synchronized and recorded using Nexus, and saved as C3D files. The motion capture files were converted to readable .trc files to ensure compatibility with OpenSim. Marker trajectory data were filtered with a low-pass Butterworth filter with a 6 Hz cutoff frequency.

The raw EMG signals were filtered using a Butterworth band-pass filter (20–400 Hz, 1st order) to remove movement artifacts and high-frequency noise. The filtered signals were rectified and low-pass filtered (6 Hz, 2nd order) to get smooth activation envelopes. Each raw muscle EMG signal was normalized by the maximum value of that specific muscle measured during the maximal sprint trial, which represented the maximum voluntary contraction [60].

To analyse EMG patterns in relation to the crank cycle, the TDC's were identified from the `CrankDistR` and `PedalR` marker trajectories. Ten full crank cycles, between 15.0 and 25.0 seconds, were extracted by identifying the highest vertical (Y) position of the pedal markers, corresponding to the TDC's.

The exact TDC timings for each condition are listed in Appendix C (Table C.3). These ten cycles were used to compute the mean and standard deviation of the EMG activation profiles.

2.4. Musculoskeletal model development

The musculoskeletal model used in this study was built in OpenSim [53], an open-source musculoskeletal modelling platform. It integrates a medial-lateral knee joint model into a lower-body musculoskeletal model used for cycling studies (Figure 2.3).

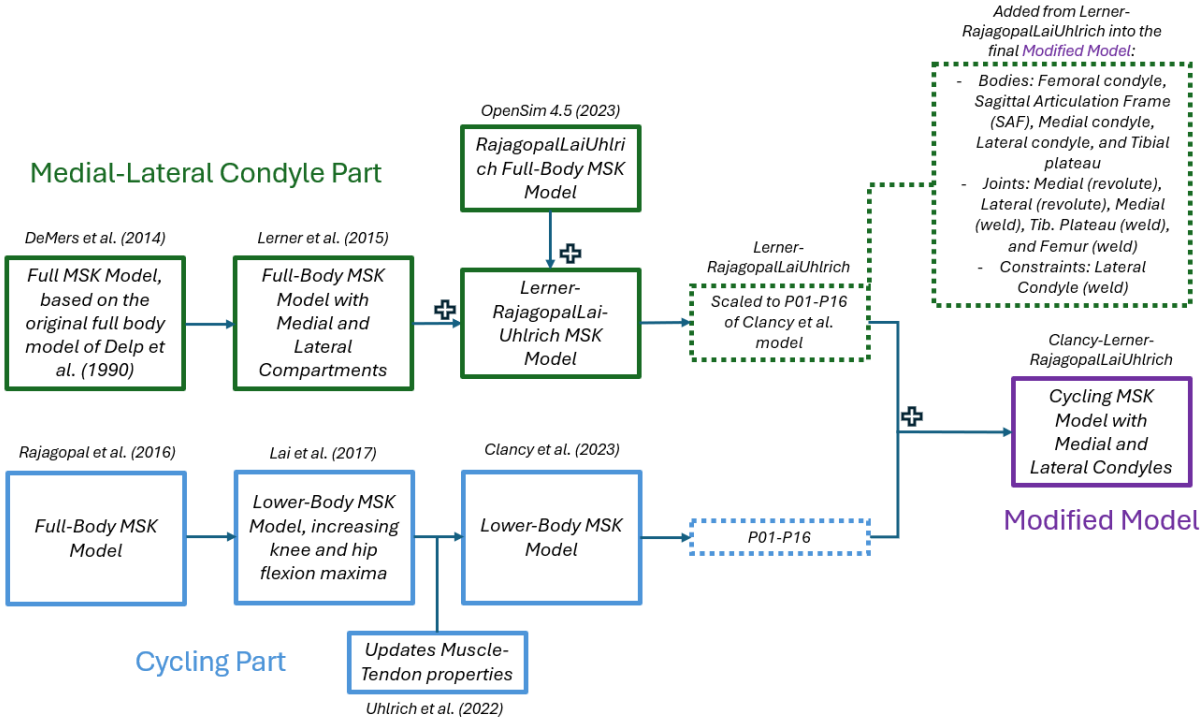

Figure 2.3: Flow chart detailing the studies used for the musculoskeletal model development methodology. The green blocks indicate the workflow of studies used for integrating the medial and lateral condyles of the knee [56]. The blue blocks indicate the workflow of studies used that resulted in the model of Clancy et al. (2023) [47], which was used as the Original Model for this study. The purple block represents the final Modified Model used in this study.

The lower-body musculoskeletal model developed by Clancy et al. [47] forms the basis of our model. It is based on the model of Lai et al. [80] which extended the Rajagopal et al. model [55] to allow larger hip (up to 120°) and knee (up to 140°) flexion ranges. Standard gait models do not account for these extreme flexion ranges, but these are typical ranges for the upstroke phase of cycling [80]. The original Clancy model includes the pelvis and lower extremities, and was designed to estimate the total TFC during cycling.

To enable compartment-specific analysis of TFC, the medial and lateral knee joint structure developed by Lerner et al. [56] (Figure 2.4) were first incorporated into the Rajagopal-Lai-Uhlrich model, which already included realistic muscle–tendon properties and high-flexion ranges. This enhanced model was then integrated into the Clancy et al. cycling model framework, enabling simulation of both total and compartment-specific KJCF during cycling.

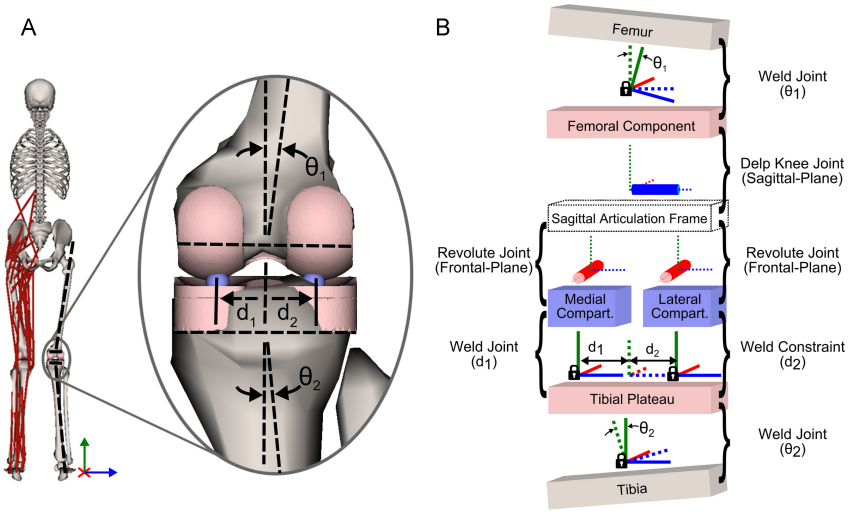

Figure 2.4: Knee model with medial and lateral condyles, adapted from Lerner et al. [56].

The knee model components (bodies, joints, and constraints) were incorporated into the original model (Figure 2.3). Before integrating the two models, the combined model of LernerRajahopalLaiUhlrich was scaled to match the subject specific model of Clancy et al.
After scaling, five bodies (`femoral_condyle`, `sagittal_articulation_frame`, `medial_compartment`, `lateral_compartment`, and `tibial_plateau`) and five joints (`femur_weld`, `medial_revolute`, `lateral_revolute`, `medial_weld`, and `tibial_plateau_weld`) were added to each leg. Finally, a weld constraint was used to attach the lateral compartment to the tibial plateau [56]. This constraint is needed, because two joints in the knee would over-constrain the model and prevent simulation. It does not matter which condyle is constrained: using a weld constraint on either of the two keeps the knee as a one-DOF joint in the sagittal plane. The two weld joints at the femur and tibia were added to model subject-specific varus/valgus angles (Figure 2.4). The `patellofemoral` and `walker_knee` joints were modified to make sure the child and parent frames were correctly adjusted to the new bodies in the knee. (Figure 2.5).

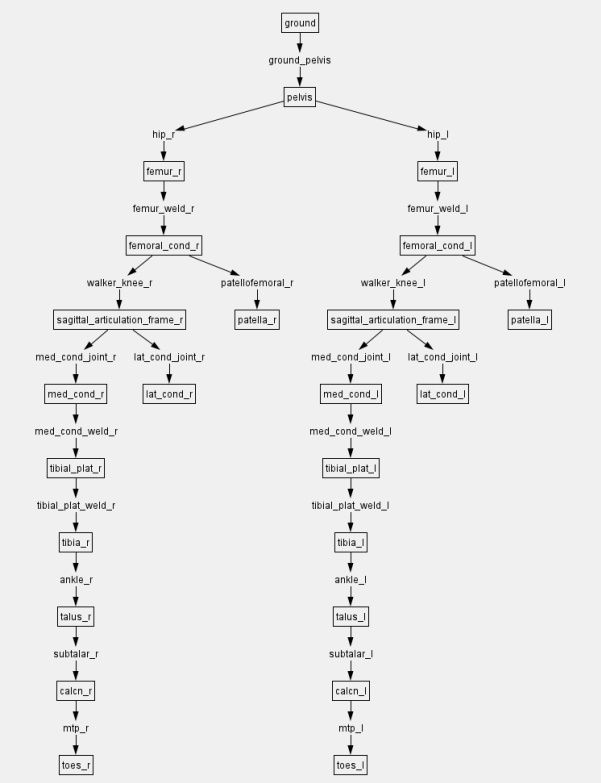

Figure 2.5: OpenSim topology of the modified model.

The Computed Muscle Control (CMC) actuators file from Rajagopal et al. [55] was used as a basis for the reserve actuator settings. To improve tracking accuracy, additional reserve actuators were added to the following coordinates: `mtp_angle_reserve`, `subtalar_angle_reserve`, `knee_angle_beta_reserve`, `med_cond_adduction_reserve`, `lat_cond_adduction_reserve` (Appendix F).
Adding reserve actuators to all model coordinates helps ensure that the system can better reproduce the experimental motion data, particularly in cases where muscle forces alone are insufficient to fully drive the model.

The cycling model of Clancy et al. implemented a pelvis-saddle interaction, to simulate a realistic mass-distribution over the bicycle [47]. Because the body weight of a biker is mainly carried by the saddle of the bike [81], six actuators are modelled at the pelvis-saddle interaction. Although upper extremities can influence lower limb muscle recruitment and joint contact forces [82, 83], especially at high power outputs [84], our study focuses exclusively on the lower extremities. Including the upper body would increase model complexity and computational cost without adding value for the steady-state, submaximal cycling conditions examined in this study.

The final modified model is a lower-limb model, with 16 DOF (6 pelvis, 3 hip, 1 knee, 1 ankle), 23 bodies, 23 joints, and 80 actuators.

2.5. Validation of the original model of Clancy et al.

2.5.1. Validation of predicted muscle activations

The processed EMG data were used to validate the original musculoskeletal model. To ensure comparability, we analysed ten consecutive crank cycles within the time window of 120-130 seconds with the same method as for EMG analysis (Section 2.3).

The original marker setup from the online dataset was used, which is different from the experimental CGM 2.4 marker model (Appendix B). The original model and the marker trajectory data served as inputs for the inverse kinematics (IK) tool in OpenSim that computes joint kinematics. Higher tracking weights were assigned to markers on bony landmarks and on the knee.

This kinematic data again served as input for the static optimisation (SO) tool, together with the PRF data [47, 62, 63] and the reserve actuator settings.

Since muscle forces cannot be measured directly, SO is used to estimate them. The human body has more muscles than DOF, so there is no unique solution to produce the required joint torques. This is known as the muscle redundancy problem. The SO tool in OpenSim estimates muscle activations by minimizing the sum of squared activations at each time step:

$$\min \sum_{i=1}^{N} a_i^2 \tag{2.1}$$

where a_i is the activation of muscle i, and N is the total number of muscles. This cost function assumes that the body chooses the most efficient coordination strategy by minimizing the overall muscle effort. Since our participants performed steady-state, sub-maximal cycling, this is a reasonable assumption and provides a good estimate of how muscles were likely activated during the task [85].

To compare the models predicted muscle activations with measured EMG, five subjects were selected from both the Gatti et al. dataset and our own experimental data, based on similar anthropometric data, cycling cadence and power output. This resulted in five comparisons between subjects from each group, where the predicted muscle activations were compared to the normalized experimental EMG data (Table 2.3).

Table 2.3: Comparison pairs of Gatti et al. and MOBI lab participants

PAIR 1:	Gatti P11	MOBI P06
Age (years)	32	25
Sex	Female	Female
Height (cm)	163.1	174.1
Weight (kg)	54.2	57.5
Cadence (RPM)	*78*	*80*
Power (W)	*94*	*100*

PAIR 2:	Gatti P03	MOBI P03
Age (years)	21	25
Sex	Male	Male
Height (cm)	171.2	176.6
Weight (kg)	74.2	76.6
Cadence (RPM)	*83*	*80*
Power (W)	*120*	*120*

PAIR 3:	Gatti P04	MOBI P10
Age (years)	23	30
Sex	Female	Female
Height (cm)	166.2	174.0
Weight (kg)	61.1	60.3
Cadence (RPM)	*92*	*90*
Power (W)	*81*	*80*

PAIR 4:	Gatti P05	MOBI P09
Age (years)	28	25
Sex	Male	Male
Height (cm)	195.4	186.3
Weight (kg)	90.8	86.3
Cadence (RPM)	*84*	*80*
Power (W)	*136*	*120*

PAIR 5:	Gatti P08	MOBI P07
Age (years)	24	25
Sex	Male	Male
Height (cm)	173.0	178.0
Weight (kg)	66.5	68.5
Cadence (RPM)	*90*	*90*
Power (W)	*117*	*120*

2.5.2. Cross-correlation analysis between EMG and model predictions

To quantitatively assess the agreement between the processed EMG signals and the muscle activation profiles predicted by both the original and modified musculoskeletal models, a cross-correlation analysis was conducted. This method quantifies the similarity in both the timing and shape of the signals, providing a more objective alternative to visual comparison of the muscle activations [86].

For each comparison pair, cross-correlation coefficients (R-values) were computed for the seven muscles measured during the experiments.

A zero-lag normalised cross-correlation from Steel et al. [87] was used, calculated as:

$$R = \frac{\sum_{i=1}^{N} x_i y_i}{\sqrt{\sum_{i=1}^{N} x_i^2} \sqrt{\sum_{i=1}^{N} y_i^2}} \tag{2.2}$$

where x_i and y_i are the respective values of the EMG and model prediction signals at time point i, and $N = 100$ represents the number of points in the normalised crank cycle.

Cross-correlation returns a value between 0 and 1, with 1 indicating perfect agreement in signal shape and timing. The calculation is mathematically equivalent to a dot product between two normalised vectors. This approach is unaffected by uniform scaling (i.e., changes in signal amplitude without altering shape) and is most sensitive to differences in timing. When timing is similar, it also captures differences in shape [86].

2.6. Verification of the modified model

To verify that the modifications to the model did not affect the estimated muscle activations and total TFC, the modified model was tested under the same conditions. The same IK settings were applied to calculate joint kinematics based on the updated model structure (Figure 2.1). Using this IK solution, SO was run, again with the same settings. The muscle activations of the modified model were compared to the ones from the original model, using the same comparison pairs (Table 2.3) and cross-correlation equation (Equation 2.2).

2.6.1. Knee joint contact force estimation

TFC was estimated using OpenSim's Joint Reaction Force (JRF) analysis tool, which computes the KJCF through a Newton–Euler approach. This integrates inverse dynamics, segmental accelerations, and muscle forces to estimate internal joint loading [87]. In this study, the total TFC was modelled as a point load acting on the tibial plateau, with the medial and lateral components acting on the respective femoral condyles.

Only the TFC was used for analysis, as compressive forces at the tibiofemoral joint represent the dominant component of the KJCF and are more clinically relevant in the context of KOA, as discussed earlier. The TFC estimated from the original model was compared to that of the updated model to verify the newly implemented modifications. Subsequently, the total TFC was distributed into medial and lateral components by determining how much of the total joint load was transmitted through each condyle [56]. These medial and lateral TFC values were used in all subsequent analyses.

3

Results

3.1. Verification of modified model

3.1.1. Muscle activations

Across all seven muscles, the modified model produced muscle activations that closely matched those of the original model (Figure 3.1). Cross-correlation coefficients between the modified and original models consistently exceeded 0.99 across all five participants and seven muscles (Table 3.1). These consistently high R-values indicate that the timing and shape of the predicted activations remained almost unchanged. This confirms that the model modifications introduced minimal differences in activation timing, supporting the robustness of the modified model.

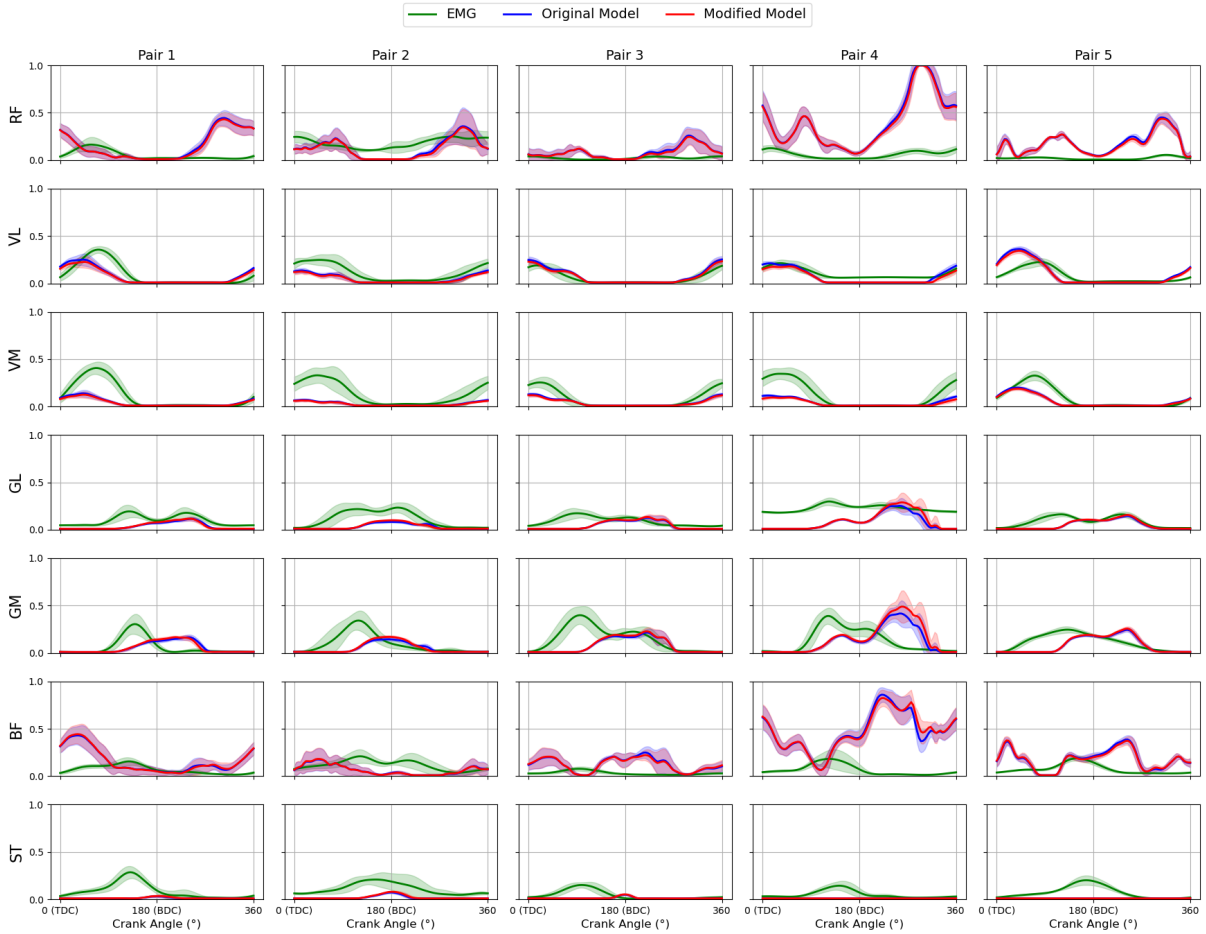

Figure 3.1: Comparison over ten consecutive cycles of simulated muscle activation and normalized EMG for comparison pairs 1 - 5. The muscles analysed are the rectus femoris (RF), vastus lateralis (VL), vastus medialis (VM), gastrocnemius lateralis (GL), gastrocnemius medialis (GM), biceps femoris (BF), and semitendinosus (ST). Shaded areas indicate one standard deviation over ten crank cycles. The green line represents the mean EMG recordings $\pm$ 1SD; the blue line shows the mean activation predicted by the original mode $\pm$ 1SD; the red line shows the mean activation predicted by the modified model $\pm$ 1SD. *Note: The high baseline activation of the GL in pair 4 is because this sensor showed visible noise during measurement.*
Pair mappings: Pair 1 – Gatti P11 & MOBI P06, Pair 2 – Gatti P03 & MOBI P03, Pair 3 – Gatti P04 & MOBI P10, Pair 4 – Gatti P05 & MOBI P09, Pair 5 – Gatti P08 & MOBI P07.

Table 3.1: Cross-correlation coefficients (R-values) comparing measured EMG to the muscle activations predicted by the original model, and the muscle activations predicted by the original model to those by the modified model.

Muscle	Pair	EMG vs. Original	Modified vs. Original
Rectus Femoris	1	0.427	0.999
	2	0.865	0.999
	3	0.738	0.998
	4	0.885	0.999
	5	0.897	0.999
Vastus Lateralis	1	0.836	1.000
	2	0.972	1.000
	3	0.985	1.000
	4	0.926	0.993
	5	0.869	1.000
Vastus Medialis	1	0.878	1.000
	2	0.966	1.000
	3	0.981	1.000
	4	0.992	0.993
	5	0.903	1.000
Gastrocnemius Lateralis	1	0.858	0.996
	2	0.881	0.992
	3	0.712	1.000
	4	0.754	0.992
	5	0.841	1.000
Gastrocnemius Medialis	1	0.487	0.990
	2	0.638	0.994
	3	0.660	1.000
	4	0.583	0.994
	5	0.741	1.000
Biceps Femoris	1	0.693	1.000
	2	0.706	0.999
	3	0.649	0.998
	4	0.515	0.998
	5	0.712	0.999
Semitendinosus	1	0.710	0.998
	2	0.868	0.998
	3	0.478	1.000
	4	0.797	1.000
	5	0.762	1.000

Pair mappings: Pair 1 – Gatti P11 & MOBI P06, Pair 2 – Gatti P03 & MOBI P03, Pair 3 – Gatti P04 & MOBI P10, Pair 4 – Gatti P05 & MOBI P09, Pair 5 – Gatti P08 & MOBI P07.

3.1.2. Total tibiofemoral compressive force

The total TFC predicted by the original and modified model showed high agreement across all five participants. The curves produced by the two models closely overlapped throughout the crank cycle, with minimal differences in shape or magnitude (Figure 3.2). Cross-correlation coefficients ranged from 0.980 to 0.998 (Table 3.2). The overlap in TFC suggests that the model modifications did not affect the overall joint loading dynamics during the crank cycle. This further verifies the musculoskeletal model modifications.

3.2. Muscle activation: EMG vs model predictions

Muscle activations predicted by the original musculoskeletal model were compared to surface EMG measurements across seven right leg lower limb muscles (Figure 3.1, Table 3.1).

The VL and VM show good agreement between EMG recordings and model-predicted activations, both in excitation timings and activation shape across all participants. This observation is supported by the consistently high cross-correlation values (Table 3.1), with R-values often exceeding 0.95.

Table 3.2: Cross-correlation coefficients (R-values) between the predicted total tibiofemoral compressive force (TFC) by the modified and the original model for each participant.

Pair	Participant	Cross-correlation ($R - value$)
1	P11	0.997
2	P03	0.992
3	P04	0.993
4	P05	0.980
5	P08	0.998

In contrast, larger discrepancies were observed for the RF, GL, GM, BF, and ST, both qualitatively (Figure 3.1) and quantitatively (Table 3.1). The GM, in particular, showed the weakest correlation with R-values ranging from 0.49 to 0.74, indicating considerable variation between predicted and measured activity. These relatively low R-values can be explained by two key mismatches: a consistent timing lag of 5–10% in the model-predicted activation, and differences in activation shape. While the model predicts a double peak for all participants, the EMG signals display only a single peak in pairs 1, 2, and 5.

The GL demonstrated a characteristic double-peak pattern in the EMG across all participants. The models replicated this pattern well in most cases, though there is again a lag of approximately 5-10%. In pair 4, visual inspection revealed noise in the EMG signal of the GL. This noise is only partly reflected in the correlation coefficient (R = 0.75), which remains relatively high despite visible distortion in the EMG signal.

The ST also showed underpredicted activations and yielded lower R-values (0.48–0.86), particularly for pairs 1 and 3, where EMG recordings showed an earlier peak in activation compared to other EMG results. While the model predicted consistent activation timing just after BDC across all participants, the EMG data showed inter-subject variability in activation onset, contributing to the reduced correlation.

Qualitatively, the RF and BF activations differed substantially between EMG and model predictions. While EMG patterns were relatively consistent across participants, and the model outputs also showed internal consistency, the mismatch between EMG and modelled activations was considerable. This mismatch was particularly evident in participant pair 4.

Both the RF and BF exhibit broad, sustained, and relatively low-amplitude activation in the EMG signals for this pair. However, the model markedly overestimates activation in both muscles, which display sharper and higher peaks. These inconsistencies may be linked to Gatti P05's higher body mass and power output during the cycling trials, which likely required different muscle recruitment patterns. The SO approach may struggle under such high-load conditions or with heavier participants, resulting in poor alignment with the EMG data from the lighter, matched participant (MOBI P09).

Further discrepancies arise in the ST activation, which is functionally synergistic with the BF. The model consistently underestimates activation in the ST while overestimating it in the BF. The cross-correlation results do not fully reflect this discrepancy, as both muscles exhibit moderate R-values. For the ST, the moderate R-values are primarily due to differences in the timing of peak activation between model predictions and EMG. In the case of the BF, moderate R-values result from the model predicting sharp, early activation peaks that do not align with the timing or shape of the EMG data, which varies substantially between participants.

3.3. Medial and lateral tibiofemoral compressive forces

There was considerable variation in peak total TFC across participants, ranging from –756 ± 127 N to –2133 ± 246 N (Table 3.3). Across all participants, the lateral TFC remained greater than the medial TFC throughout most of the crank cycle (Figure 3.3). This suggests that during cycling, the lateral condyle contributes more to the total compressive load than the medial condyle. On average, the lateral TFC was –837 N, compared to –513 N in the medial compartment (Table 3.3).

A primary peak in total TFC is observed just after TDC, consistent across participants and aligned with expectations based on the power phase of cycling. In pair 4, a second peak appears just after BDC, which is barely seen in other participants. This additional peak likely results from the elevated muscle activity of RF and BF during this phase of the crank cycle (Figure 3.1, Section 3.2).

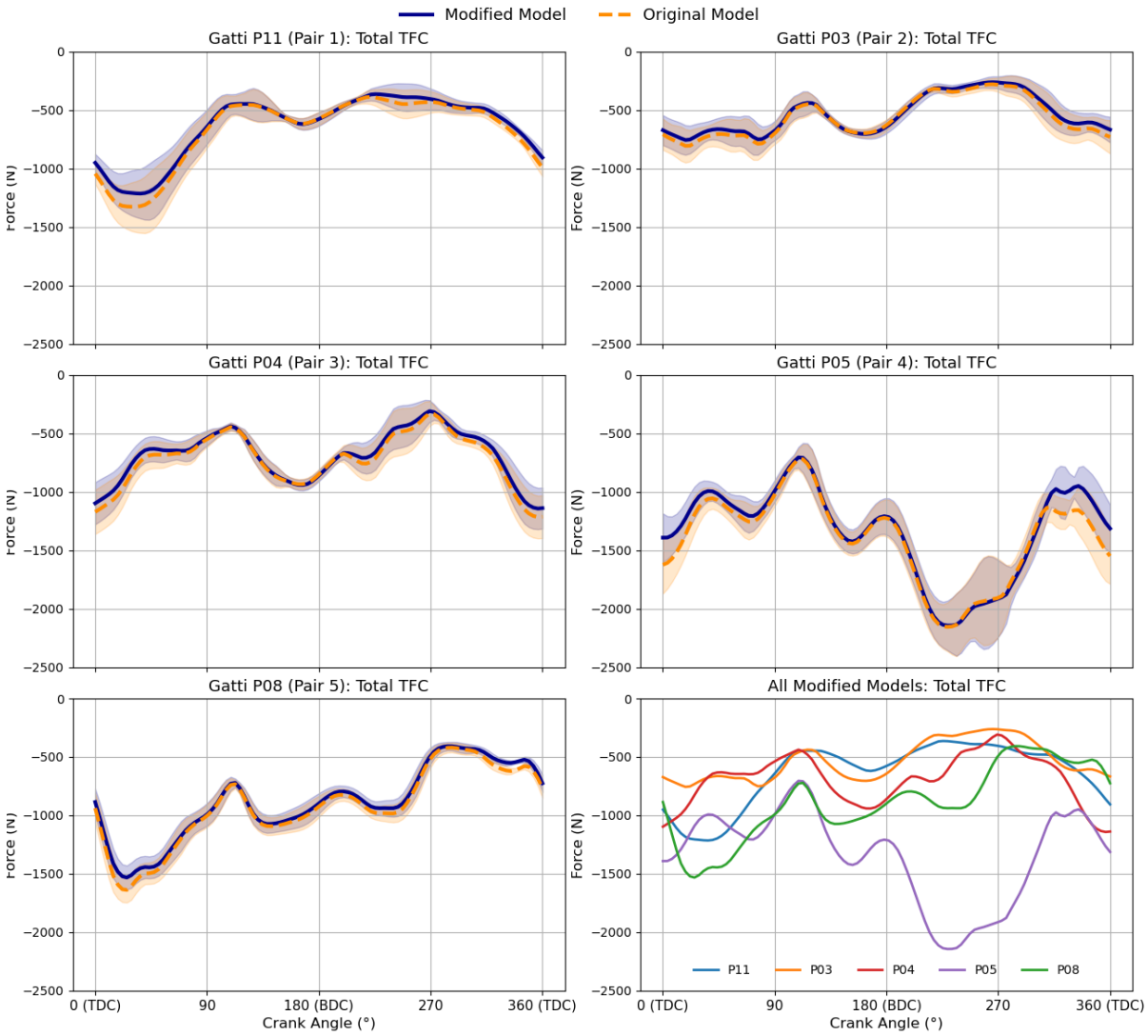

Figure 3.2: Total tibiofemoral compressive force (TFC), expressed in the tibial (child) frame. The plots show the mean TFC ± 1SD over ten consecutive crank cycles for each participant, comparing the modified model (solid blue) and the original model by Clancy et al. (dashed orange). The bottom right subplot shows the total TFC curves for all participants using the modified model, highlighting inter-individual variability in magnitude and timing across the crank cycle.

A smaller local peak in total TFC is observed at BDC across all participants. Although the magnitude of this peak varies, it is most pronounced in pairs 3, 4, and 5 (P04, P05, and P08). In these participants, the lateral TFC component deviates substantially from the medial component around BDC, indicating asymmetrical tibiofemoral joint loading (Figure 3.3). These lateral-dominant fluctuations influence the shape of the total TFC profile during this phase and may reflect subject-specific differences in pedalling mechanics or neuromuscular coordination. These differences are consistent with earlier observations of inter-subject variability in muscle activation patterns, particularly in the BF, which has a notable influence on lateral TFC.

The total TFC represents the direct sum of the medial and lateral components at each point in the crank cycle for all participants. This confirms that total TFC is represented as the sum of medial and lateral components at each crank angle.

Table 3.3: Peak total tibiofemoral compressive force (TFC) for each participant (± SD), along with the corresponding medial and lateral TFC values at the time of peak total TFC. The final row shows the average across all five participants.

Participant	Pair	Total TFC (N)	Medial TFC (N)	Lateral TFC (N)
P11	1	-1216 ± 212	-491 ± 77	-725 ± 136
P03	2	-756 ± 127	-334 ± 46	-422 ± 83
P04	3	-1113 ± 184	-465 ± 66	-648 ± 120
P05	4	-2133 ± 246	-656 ± 90	-1477 ± 184
P08	5	-1533 ± 101	-621 ± 37	-912 ± 64
Average	–	-1350	-513	-837

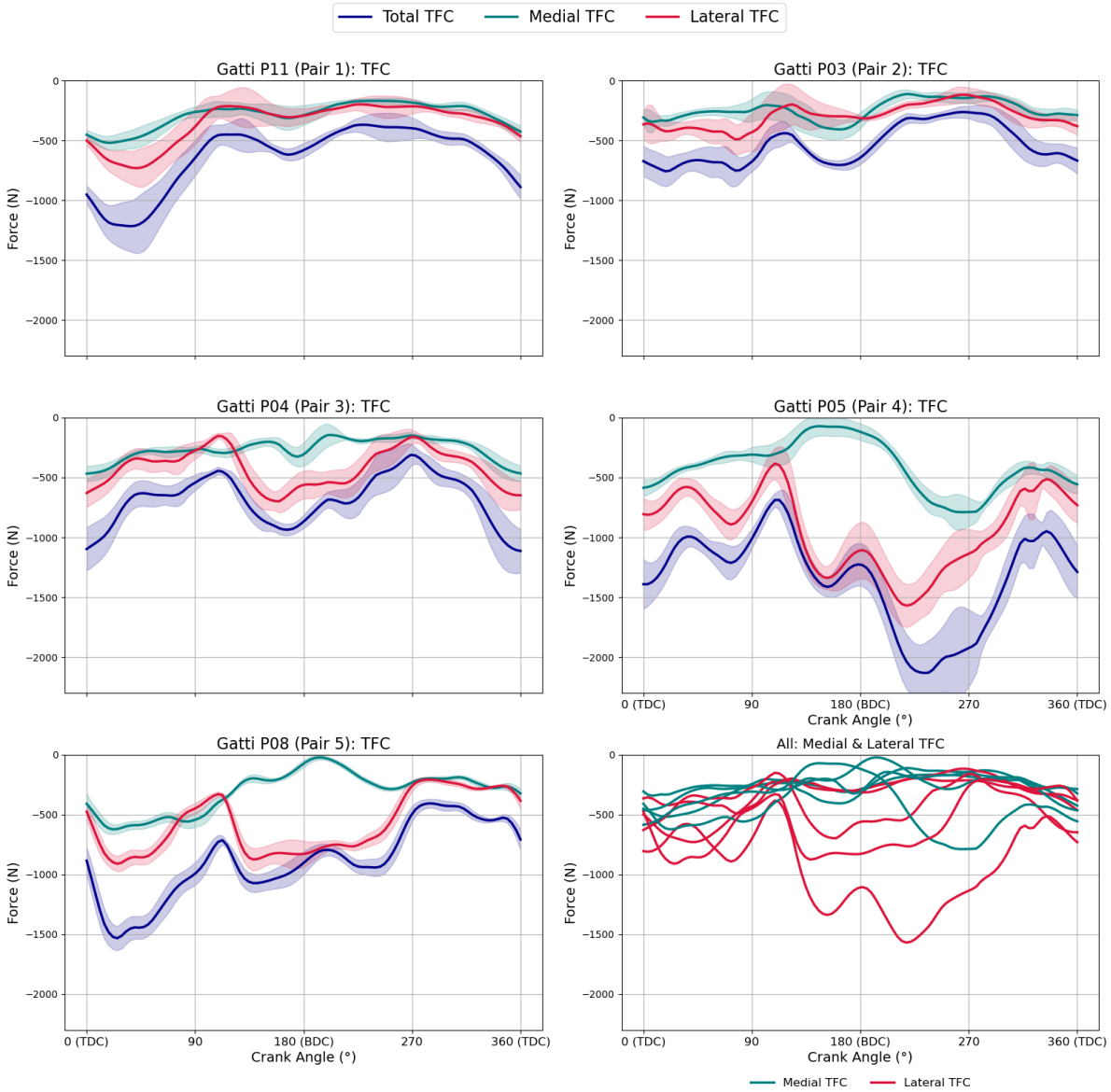

Figure 3.3: Tibiofemoral compressive force (TFC) for all comparison pairs, expressed in the tibial (child) frame. Each plot shows the mean ± SD of total (blue), medial (cyan), and lateral (pink) TFC over ten consecutive crank cycles. The bottom-right subplot presents the medial and lateral TFC curves for all participants individually, highlighting consistent lateral loading dominance and inter-subject variability in joint load distribution throughout the crank cycle.

4

Discussion

This study combined musculoskeletal modelling with experimental data to estimate the TFC and their distribution across the medial and lateral condyle during cycling. The primary goal was to validate an existing musculoskeletal model by Clancy et al. [47] and enhance its knee complexity by incorporating medial and lateral condyles. The development of the laboratory environment demonstrates a strong potential for future in-hospital cycling research. The modified musculoskeletal model produced results consistent with the original model, while the added complexity to the knee joint provided novel insights into the distribution of TFC, such as consistently higher loads observed on the lateral condyle.

4.1. Modified musculoskeletal model

4.1.1. Verification

The modified model showed very similar muscle activation patterns ($R > 0.99$) and total TFC ($R > 0.98$) compared to the original model. The minor differences are mainly due to added joint constraints and small knee and patellofemoral joint alignment translations. In particular, changes to the parent frames of certain joints may have caused slight alterations in joint positioning.

4.1.2. Model performance compared to EMG

Muscle excitation timing

The predicted muscle excitation timings differed from the EMG data, particularly for the gastrocnemius muscles (GL and GM), where modelled activation lagged by approximately 5–10%. This is consistent with previous findings [80]. Several factors may explain these discrepancies. First, the two datasets included different subjects with potentially varying cycling techniques and neuromuscular control strategies. Although cadences and power outputs were matched closely between datasets, the minor differences could be a reason for significant differences in muscle excitation.

Second, differences in bike fitting between the datasets, such as saddle height and overall bike setup, likely influenced joint kinematics, particularly hip and knee flexion angles (Appendix I). These kinematic variations can affect joint moments and muscle recruitment, directly impacting the estimated KJCFs.

Moreover, in cycling, the downward force of one leg passively contributes to lifting the opposite pedal during the upstroke. This mechanical interdependence reduces the need for active muscle effort in the pulling leg. However, the model treats each leg's motion independently and does not account for this passive assistance. As a result, it likely overestimates muscle activation during the pull phase, particularly in hip and knee flexors that would not need to generate as much force under realistic conditions.

Passive force omission

SO does not model passive forces or activation dynamics [88]. Passive muscle forces are generated from the tissue's mechanical properties, such as muscle fibres and connective tissue tension. Unlike active forces, passive forces do not require metabolic energy to produce force [89]. The activation dynamics represent the physiological delay between neural excitation and the muscle force development [67, 90]. The absence of passive force modelling and activation dynamics in SO impacts the timing and magnitude of predicted activations, reducing physiological realism [67]. In addition, EMG signals are

subject to processing delays and signal noise and reflect neural excitation rather than muscle activation, making direct comparison with SO outputs challenging.

In the absence of passive force modelling, SO relies solely on active muscle forces to generate joint torques. This limitation leads to higher simulated muscle activations compared to those observed in EMG data. For example, passive forces typically assist with hip flexion ($\pm$ 80°) around TDC [47], and their omission requires compensatory higher activations of hip flexors and synergistic muscles, altering physiological muscle recruitment patterns, such as the activation of the RF or the iliopsoas muscles.

When iliopsoas activation approaches its maximum capacity (Appendix G), the RF compensates by activating more than is physiologically realistic (Figure 3.1). However, since the RF is also a knee extensor, this leads to unintended knee extension torque at a time when the knee should remain flexed (approximately between 270° and 360° crank angle) [91]. This, in turn, leads to additional activation of knee flexors such as the BF to counteract the extension torque, creating artificial co-contraction and increasing the modelled TFC. This co-contraction elevates the TFC, a pattern consistent with prior simulation studies [43], but is not observed in experimental EMG data. In the EMG data, the RF shows minimal activity during this phase of the cycle (Figure 3.1, Figure 3.3).

Maximal isometric force

Maximal isometric force (MIF) in OpenSim is a parameter representing a muscle's force-generating capacity, which is proportional to its physiological cross-sectional area (PCSA). The musculoskeletal model used in this study assigns identical MIF to all subjects, irrespective of differences in body mass or segmental inertia [47]. For example, the RF muscle is assigned a fixed MIF of 2192 N. Although anthropometric scaling adjusts limb dimensions, muscle strength properties are not individually adapted. As a result, heavier individuals require greater RF muscle activation to achieve hip flexion during cycling, as previously observed by Michaud et al. [92].

Reserve actuator activation

When maximal activation is reached and is still insufficient to meet the required torque, the model resorts to reserve actuators to enforce the kinematics (Appendix G). This compensation is particularly evident in pair 4, where participant P05 from the online dataset exhibits abnormally high RF and BF activations, accompanied by elevated reserve actuator activity during the upstroke phase. In contrast, participants P11, P03, P04, and P08 show reserve actuator usage within normal ranges (Appendix G) [67]. This suggests that the abnormal reserve actuators use primarily results from the heavier body mass and insufficient passive support in P05.

Monoarticular vs. biarticular muscles

The closer match (R = 0.84 - 0.99) for monoarticular muscles (VM and VL) suggests that SO approaches can accurately predict muscles primarily acting at a single joint, whereas the biarticular muscles (RF, GM, GL, BF, and ST), involved in multi-joint coordination and dynamic control, are less accurately represented (R = 0.43 - 0.90). The VM and VL exhibited more straightforward and consistent activation patterns, reflecting their primary role in generating knee extension torque. In contrast, the activation patterns of biarticular muscles were more variable across subjects and crank positions. This greater variability likely reflects the complex functional role of biarticular muscles in regulating the distribution of net joint moments and external force directions during cycling [93].

Muscle redundancy problem

Different motor control strategies can activate different muscles (muscle redundancy problem), potentially leading to variations in KJCF, even when kinematics and kinetics remain the same. This may explain the differences observed in the EMG data between participants. This raises questions about the reliability of SO approaches in cycling [27]. The SO method used in this study minimizes the sum of squared muscle activations (Equation 2.1), treating all muscles equally in the cost function. For example, ST has a smaller MIF (591 N) compared to other muscles that contribute to hip extension, such as the BF (1313 N) and semimembranosus (2201 N). As a result, it is typically recruited later, which explains its lower peak activation and delayed excitation. This pattern of size-based recruitment may also affect other muscles during cycling, although the effects might be less pronounced than in the case of the ST.

4.1.3. Internal validation

Inter-subject variability

There is considerable inter-subject variability for the EMG measurements and the model predictions. The five participants cycled at different cadences and power outputs, which affected joint loading and muscle demand. These differences led to noticeable variations in predicted muscle activation patterns and KJCF.

EMG performance

We observed a muscle recruitment pattern in which peak activation occurred first in the RF, followed by the vastii muscles, then the hamstrings (ST and BF), and finally, the gastrocnemii muscles. This sequence is consistent with findings from previous studies [34, 65, 94, 95, 96, 97].

The GL consistently exhibited a double-peak activation pattern across all participants in the EMG recordings and model predictions. Although a timing lag of approximately 5–10% was observed, the shape of the predicted activation aligned well with the measured data. This consistency suggests a relatively stable neuromuscular strategy for GL across subjects. By comparison, the GM showed greater variability in EMG profiles. Some participants (pairs 3 and 4) displayed a double peak pattern, whereas others (pairs 1, 2, and 5) showed only a single, more dominant peak just before BDC (Figure 3.1).

The first peak, located just before BDC, likely corresponds to plantarflexion during the power phase of the pedal stroke. The presence of a second peak in some participants may be linked to knee flexion during the upstroke, indicating inter-individual differences in muscle coordination strategies. This interpretation is consistent with prior observations that activation around BDC in the hamstrings and gastrocnemii can be associated with a backward-pushing motion, which may vary between individuals depending on their cycling technique [97].

The higher overall EMG amplitude observed for GM, compared to GL, aligns with its greater PCSA, as previously reported [98]. This anatomical distinction likely contributes not only to its force-generating potential but also to the variability in its activation shape and magnitude across subjects.

Finally, the observed differences between GM and GL activation patterns underscore their distinct neuromechanical roles and control profiles [98]. While the GL appears to follow a more uniform activation strategy across participants, the GM seems to be more sensitive to variations in individual cycling technique, joint kinematics, or motor control preferences. These findings reinforce the importance of considering both anatomical and neuromotor factors when interpreting inter-subject variability in EMG data.

Static optimisation performance

The predicted muscle activations using SO show good agreement with earlier modelling studies. In particular, the excitation and activation patterns are consistent with the SO-based predictions reported by Menard et al. [43] and with CMC outputs from Lai et al. [80]. Clancy et al. [47] used the OpenSim Moco tool to generate muscle-driven simulations to estimate muscle forces, which is a different approach than in this study (Appendix K). However, similar muscle activations were observed, consistent with other direct collocation methods [99].

4.2. Knee joint contact force estimation

4.2.1. Total tibiofemoral compressive force

Peak total TFC force magnitudes varied considerably across the five participants (Table 3.3). The group mean peak TFC of 1350 N aligns well with values reported in previous simulation and musculoskeletal modelling studies [34, 46, 47, 62]. The two participants cycling at 80 and 100 W exhibited peak TFC values that closely correspond to those measured in vivo using instrumented joint implants under similar conditions (75–95 W) [22].

Muscle forces are the primary contributors to TFC and other KJCF [100, 101]. Previous studies have shown that fluctuations in muscle force patterns can significantly affect the magnitude of the KJCF [102]. In particular, peak TFC has been closely associated with the force output of knee flexor muscles, mainly the BF [43]. This trend is also evident in our results, where increased BF activity corresponds with higher TFC values. This is specifically visible for participant P05 (pair 4).

In general, higher power outputs correspond with higher measured PRF and muscle activations, leading to increased joint moments and TFC. Peak TFC magnitudes are observed in participants P05 and P08

(Table 3.3), exhibiting higher knee and ankle flexion moments and a pronounced hip abduction moment (Appendix J). Participant P03, who cycled at a similar cadence and power output but showed the lowest peak TFC, is particularly interesting. This is likely explained by a combination of more efficient pedalling mechanics (Figure J.2) and lower joint moments, which are linked to reduced muscle activations. P03 also shows lower hip flexion angles (Appendix I), which is associated with reduced model-predicted activations of the VM, VL, RF, and BF (Figure 3.1, pair 2), as also noted by Dorel et al. [103]. Around BDC, BF activation is particularly low compared to other participants, likely because the more extended hip position places the muscle in a lengthened state with reduced mechanical advantage, limiting its contribution to hip extension. This pattern aligns with the lower TFC observed in P03, making them a clear outlier in the group with a plausible biomechanical explanation.

4.2.2. Medial and lateral tibiofemoral compressive force

Across all participants, the lateral condyle contributed more to the total TFC than the medial condyle. This is interesting, as in gait analysis, this is the other way around [104, 105]. The VL shows higher activation than the VM, which aligns with its substantially greater MIF (5149 N vs. 2748 N). Furthermore, the GL is less activated than the medial head, which is consistent with the higher MIF of the GM (3116 N vs. 1575 N). This suggests that muscle activation patterns generally reflect the force-generating capacity of the individual muscles, as expected from the cost function (Equation 2.1). Overall, the greater strength of the VL indicates that more force is likely transmitted through the lateral side of the knee, potentially influencing TFC distribution.

4.3. Limitations

4.3.1. Musculoskeletal model

Comparability

When analysing the comparison between the EMG results and the model's predicted muscle activations (Chapter 3, Figure 3.1), it should be noted that these data were collected from different subjects, cycling under slightly different conditions, on different bike setups, and in separate laboratory environments. Likewise, conclusions about the generalisability of the TFC results (Chapter 3, Figure 3.3) must consider that subjects in pairs 1–5 cycled at varying cadences (80 or 90 RPM) and power outputs (80, 100, or 120 W). Future studies should use EMG and model-predicted data from the same subjects cycling under identical conditions and in the same controlled environment to improve comparability. Consequently, full validation of the model predictions against EMG data was constrained by the methodological differences in this study.

In addition, the cross-correlation used to quantify the similarity in muscle activation should be interpreted cautiously. The method is sensitive to excitation timing but also influenced by signal characteristics such as low overall activation or unfiltered noise. When the EMG or the predicted muscle activation remains near zero, the R-value may still appear high. Likewise, unfiltered noise in the EMG signal can inflate the correlation, giving a misleading impression of agreement with the model prediction.
Finally, only five comparison pairs were available for analysis, which limits the strength of the findings. While clear trends were observed, the small sample size prevents definitive conclusions from being drawn based on this study alone.

Musculoskeletal model

The original model is based on a 75-kg and 170-cm tall male subject [55]. This model does not accurately represent every subject of the study. Particularly female subjects, whose bony structure and muscle properties differ from those of male subjects [106]. Model personalisation was limited to anthropometric scaling of this male reference model [43]. Current studies are working on personalised models, including better representation of the female musculoskeletal systems [107].

Motion capture and soft tissue artefacts

Kinematic data were obtained through skin-mounted markers, which are prone to soft tissue artefacts (STA) [108, 109, 110]. These artefacts, caused by skin and muscle motion relative to the underlying bone, introduce errors in joint angle estimation, particularly in dynamic movements like cycling. This affects the accuracy of IK, and therefore of SO and KJCF estimation. STA tend to be more severe in individuals with higher BMI [111], which is especially relevant in clinical populations such as people with KOA. While standard filtering techniques reduce noise, they cannot fully eliminate STA. New approaches that minimize the influence of STA, such as the MiKneeSoTA approach [110], could lead to more precise

measurements of knee joint rotations and translation. Furthermore, accurate bone tracking methods such as fluoroscopy may be needed to improve the validity of kinematic input in future studies.

1-DOF knee model

The model used a knee joint with one degree of freedom (DOF), representing flexion-extension (FE) in the sagittal plane, consistent with other studies [47, 55, 80]. Although the model adds anatomical detail via medial and lateral condyles, the knee model used in this study is still constrained to a single movement plane. In reality, the knee functions as a six DOF joint. To better match *in-vivo* measurements, the DOF should be increased to three. Recent research shows that a three-DOF knee model, capable of FE, internal-external (IE), and abduction-adduction (Abd-Add), improves physiological accuracy [112].

Tibiofemoral shear forces

The model used in this study does not estimate the tibiofemoral shear force (TFS). In the original knee model used for this study [56], TFS was also not reported. This is a critical omission, as shear forces may contribute significantly to cartilage degeneration and KOA progression [113, 114, 115, 116]. Although TFS is generally the smallest component of KJCF [22, 38], their association with cartilage shear stress and degeneration suggests they may play a more influential role than previously assumed [117]. The absence of shear force analysis during cycling, especially given the dynamic loading patterns, leaves a crucial gap in our understanding of how cycling affects knee joint mechanics.

In the model setup, the medial condyle was connected to the tibial plateau using a weld joint, while the lateral condyle was attached via a weld constraint. In this configuration, all shear forces were transmitted through the medial side, with no force distributed through the lateral condyle. When the setup was reversed (applying the weld joint to the lateral condyle and the weld constraint to the medial), the entire shear load shifted to the lateral side. This indicates that weld constraints could not transmit shear forces, whereas weld joints could do this. Due to this limitation in the model's force distribution mechanics, TFS could not be reliably analysed and was therefore excluded from the scope of this thesis.

Optimisation

As discussed, SO disregards activation dynamics and passive muscle fibre forces [88], potentially limiting physiological realism [67]. This study employed the baseline cost function of SO (Equation 2.1), which minimizes the sum of squared muscle activations, treating all muscles equally. In contrast, Clancy et al. [47] proposed an enhanced approach by incorporating an additional objective to minimize TFC. Their results significantly improved the accuracy of predicted joint contact forces.

Similarly, Gatti et al. [62] presented an alternative strategy by assigning different weighting factors to individual muscles during optimisation (Equation 4.1).

$$\min \sum_{i=1}^{N} c_i a_i^2 \tag{4.1}$$

where c_i is an integer weighting constant for each muscle, a_i is the activation of muscle i, and N is the total number of muscles [87].

While most muscles in the method of Gatti et al. [62] retained a weighting factor of one, the hamstrings and gastrocnemii muscles were weighted by factors of three and seven, respectively. This adjustment allowed the optimisation to reproduce experimentally measured muscle activation patterns more accurately. Implementing a similar weighted optimisation approach may enhance the agreement between predicted and experimental EMG data, particularly for muscles that span two joints (bi-articular), which have shown to be challenging to model accurately.

4.3.2. Experimental setup: MOBI lab

This study was conducted under controlled conditions at the Motion Biomechanics and Imaging (MOBI) lab in the Erasmus Medical Center to ensure reproducibility.

Participants

We recruited healthy participants for this concept study to establish a baseline under controlled conditions. Although cycling is widely prescribed in rehabilitation for individuals with KOA, there is limited data on their cycling biomechanics. In gait, KOA patients show distinct kinematic and kinetic patterns compared to healthy individuals [118], suggesting that similar differences may also appear during cycling.

This underlines the need for future research involving KOA populations to inform clinical applications accurately.

Experimental protocol

This study uses a crank arm length of 172.5 mm, which is a standard length [70]. Although variations in crank length can influence biomechanical factors, such as hip and knee flexion angles, minor adjustments (approximately 5 mm) are unlikely to significantly impact the study's outcomes [119] and are therefore not investigated.

Cadence and power output were recorded using the Garmin Connect app [79], which provides data per second. However, for detailed biomechanical analysis, higher-resolution data is preferred. Since kinematic and PRF data are available per frame, having cadence and power output at the same resolution would allow a better understanding of how moment-to-moment changes in force and movement influence mechanical output.

Saddle and handlebar heights were set consistently across participants, but the exact measurements were not noted. This means the setup cannot be reconstructed accurately from the marker data, limiting reproducibility and the ability to compare setups across participants or sessions.

The EMG data were normalised using the maximal sprint trial. However, this trial was performed at a fixed power output of 200 watts. During the experiments, it became clear that most participants struggled more with the high cadences than the power output. As a result, the trial likely did not represent aan actual maximal voluntary contraction for all muscles.

4.4. Future work

This study was built on the work of Clancy et al. [47], who were among the first in cycling biomechanics to freely share their musculoskeletal models and the kinematic and kinetic data. This open collaboration sets a standard for future work. Future research should prioritise sharing their data to enhance our understanding of cycling biomechanics, enabling others to validate findings and improve models.

4.4.1. Musculoskeletal model

Solver

Future work regarding the musculoskeletal model should consider another optimisation tool which does not disregard passive forces and activation dynamics. A different type of solver that is already widely used in OpenSim and includes passive forces is Computed Muscle Control (CMC). This solver is, however, computationally expensive [120]. A promising alternative is the Residual Muscle Reduction (RMR) solver, currently being developed by Belli et al. [88]. The RMR solver incorporates constraints on JRF as explicit linear functions of muscle activations, directly modelling joint stability. Furthermore, RMR is computationally more efficient than CMC and considers passive forces and activation dynamics.

EMG-informed musculoskeletal modelling

Another key improvement involves the use of EMG-informed musculoskeletal models. As discussed in Chapter 3.2, the predicted muscle activations did not fully match the experimental EMG data. Since muscle activation directly influences joint loading, EMG-informed approaches will likely offer more accurate and subject-specific estimations. These models can better account for co-contraction [121] and variability in muscle recruitment strategies. Recent studies, including in cycling [27], support this direction. Future studies could benefit from adopting EMG-informed modelling approaches, which may offer more physiologically realistic muscle force estimations than SO [122].

Increasing DOF knee model

Future work should explore implementing a three-DOF knee joint model to improve the physiological accuracy of joint mechanics. Recent developments, such as the ellipsoidal bi-condylar model by Hörmann et al. [112], enable FE, IE rotation, and Abd-Abb by modelling the medial and lateral condyles separately based on anatomical geometry. This approach improves alignment with *in vivo* fluoroscopic data without requiring the complexity of the full six-DOF models. Integrating such a model would allow for more realistic KJCF estimations, especially in the context of patient-specific knee anatomy, where differences in bone- shape and alignment influence how forces are distributed across the joint. Future studies should test whether this modelling approach can resolve the limitations in TFS estimation identified in this study.

Outside laboratory measurements

Experiments can only be done within a laboratory setting, and future work should explore ways to move outside of the laboratory environment as well. Recent studies show the potential of estimating PRF with a machine learning model based on the crank angle, cadence, power output, and participant's weight and height [123]. In parallel, smartphone-based motion capture systems such as OpenCap are becoming increasingly advanced [124]. However, these approaches are not yet accurate enough to estimate personalised KJCF. Further research is needed to improve the accuracy before they can replace laboratory settings.

4.4.2. Towards a hospital-based cycling laboratory

Several methodological improvements are recommended to improve the reproducibility and accuracy of future cycling studies in the laboratory.

First, the laboratory setup should be thoroughly documented. A standardised protocol for bike configuration is essential, including accurate measurements of saddle height and handlebar position. Additionally, markers should be placed on the bike frame itself to precisely track the bike's position and orientation in space across trials. Feet should always be securely attached to the pedals, preferably clipless shoes, to minimise unwanted foot motion in the medial-lateral and anterior-posterior directions. This attachment should position the ball of the foot over the centre of the pedal, following best-practice guidelines [72].

Future studies should use pedals capable of measuring three-DOF forces and moments. Instrumented pedals would enable the direct comparison of model-predicted muscle activations with EMG data from the same trial, overcoming the limitations in cross-subject comparisons encountered in this study. Furthermore, kinematic and kinetic data should be time-synchronised, ideally with automated triggering when a specific marker position is detected (i.e. when the crank reaches TDC).

A combination with fluoroscopy is proposed to increase accuracy further and go behind conventional motion capture. Combining motion capture with fluoroscopy provides a more accurate assessment of joint kinematics by overcoming the STA associated with motion capture alone [125]. This combination could allow for precise measurement of bone movements during cycling, especially in early-stage KOA. Importantly, knee anatomy varies considerably between individuals [126], limiting biomechanical findings' generalisability. A combined modelling approach, using fluoroscopy, musculoskeletal modelling, and finite element method (FEM) simulations, could provide a more personalised understanding of joint loading. Finally, in an ideal initial test setup, patients with knee implants fitted with strain gauges could provide ground-truth force data, closing the loop between simulation and reality.

Ultimately, we propose the development of a hospital-based cycling laboratory where patients can undergo biomechanical assessment and receive personalised rehabilitation guidance. Conducting the study within a hospital setting would allow patients to complete data collection and evaluation in a single visit, reducing clinical burden. The lab would combine kinematic, kinetic, EMG, and anthropometric measurements for patient-specific analysis. Such a setup would bridge the gap between biomechanical research and clinical application, supporting more targeted and effective rehabilitation strategies.

5

Conclusion

This thesis contributes to the development of a novel musculoskeletal cycling model that estimates compartment-specific KJCF. Building upon the model proposed by Clancy et al. [47], and incorporating anatomically distinct medial and lateral condyles adapted from Lerner et al. [56], this work enables the first estimations of TFC distribution across the knee joint during cycling. The analysis of compartmental load distribution offers new insights into the potential role of cycling in mitigating the progression of condyle-specific KOA. Furthermore, this study lays the groundwork for more cycling research in clinical environments, potentially complementing gait analysis within biomechanical rehabilitation programs.

The modified model maintained performance comparable to the original model, achieving cross-correlation values over 0.99 for predicted muscle activations and producing similar total TFC estimates. Validation of the model predictions against EMG data showed strong agreement for the VL ($R = 0.84–0.99$) and VM ($R = 0.88–0.99$), while larger discrepancies were observed for the bi-articular muscles. Full validation of the model predictions against EMG data was therefore not possible, as differences in subjects, methodology, and experimental conditions limited direct comparability.

Notably, this study is the first to demonstrate that cycling consistently loads the lateral condyle more than the medial condyle across all participants, in contrast to well-established gait loading patterns. This novel finding may reshape how cycling is applied in rehabilitation, providing a potential low-impact intervention strategy to target compartment-specific KOA. The experimental setup developed for this study was successfully implemented across eleven sessions, confirming the feasibility of conducting controlled cycling studies with kinematic and EMG data.

While the model relied on simplified joint mechanics, static optimisation, and only five comparison pairs analysis, these limitations are acknowledged and provide direction for future studies. Recommended improvements include adopting other (EMG-informed) solvers, integrating additional degrees of freedom in the knee, and enhancing subject-specific modelling. These efforts will be crucial in advancing towards a hospital-based cycling laboratory capable of delivering personalised KJCF profiles.

In conclusion, this research presents an important first step towards clinical cycling studies that account for compartment-specific TFC estimation. These early findings form the foundation for future research, both in terms of musculoskeletal model refinement and targeted clinical applications.

References

[1] Tuhina Neogi and Yuqing Zhang. “Epidemiology of OA”. *Rheumatic diseases clinics of North America* 39.1 (Feb. 2013), pp. 1–19. ISSN: 0889-857X. DOI: 10.1016/j.rdc.2012.10.004.

[2] Jaimie D. Steinmetz et al. “Global, regional, and national burden of osteoarthritis, 1990–2020 and projections to 2050: a systematic analysis for the Global Burden of Disease Study 2021”. *The Lancet Rheumatology* 5.9 (Sept. 2023). Publisher: Elsevier, e508–e522. ISSN: 2665-9913. DOI: 10.1016/S2665-9913(23)00163-7.

[3] Alexander Merritt et al. “Frequency of MRI-detected peripheral osteoarthritis in athletes during the Summer Olympics in Rio 2016”. *Osteoarthritis and Cartilage Open* 3.4 (Dec. 2021). Publisher: Elsevier. ISSN: 2665-9131. DOI: 10.1016/j.ocarto.2021.100199.

[4] Amanda J. Salacinski et al. “The Effects of Group Cycling on Gait and Pain-Related Disability in Individuals With Mild-to-Moderate Knee Osteoarthritis: A Randomized Controlled Trial”. *Journal of Orthopaedic & Sports Physical Therapy* 42.12 (Dec. 2012). Publisher: Journal of Orthopaedic & Sports Physical Therapy, pp. 985–995. ISSN: 0190-6011. DOI: 10.2519/jospt.2012.3813.

[5] Aiyong Cui et al. “Global, regional prevalence, incidence and risk factors of knee osteoarthritis in population-based studies”. *EClinicalMedicine* 29-30 (Dec. 2020), p. 100587. ISSN: 2589-5370. DOI: 10.1016/j.eclinm.2020.100587.

[6] Reva C. Lawrence et al. “Estimates of the prevalence of arthritis and other rheumatic conditions in the United States: Part II”. *Arthritis & Rheumatism* 58.1 (2008), pp. 26–35. ISSN: 1529-0131. DOI: 10.1002/art.23176.

[7] Joern W.-P. Michael, Klaus U Schlüter-Brust, and Peer Eysel. “The Epidemiology, Etiology, Diagnosis, and Treatment of Osteoarthritis of the Knee”. *Deutsches Arzteblatt International* 107.9 (Mar. 2010), pp. 152–162. ISSN: 1866-0452. DOI: 10.3238/arztebl.2010.0152.

[8] Thomas P. Andriacchi, Seungbum Koo, and Sean F. Scanlan. “Gait Mechanics Influence Healthy Cartilage Morphology and Osteoarthritis of the Knee”. *The Journal of Bone and Joint Surgery. American volume.* 91.Suppl 1 (Feb. 2009), pp. 95–101. ISSN: 0021-9355. DOI: 10.2106/JBJS.H.01408.

[9] J. Wei et al. “Risk factor heterogeneity for medial and lateral compartment knee osteoarthritis: analysis of two prospective cohorts”. *Osteoarthritis and Cartilage* 27.4 (Apr. 2019). Publisher: Elsevier, pp. 603–610. ISSN: 1063-4584, 1522-9653. DOI: 10.1016/j.joca.2018.12.013.

[10] O. D. Schipplein and T. P. Andriacchi. “Interaction between active and passive knee stabilizers during level walking”. *Journal of Orthopaedic Research* 9.1 (1991), pp. 113–119. ISSN: 1554-527X. DOI: 10.1002/jor.1100090114.

[11] Jacob K. Gardner et al. “Effects of toe-in angles on knee biomechanics in cycling of patients with medial knee osteoarthritis”. *Clinical Biomechanics* 30.3 (Mar. 2015), pp. 276–282. ISSN: 0268-0033. DOI: 10.1016/j.clinbiomech.2015.01.003.

[12] Barton L. Wise et al. “Patterns of compartment involvement in tibiofemoral osteoarthritis in men and women and in whites and African Americans”. *Arthritis Care & Research* 64.6 (2012), pp. 847–852. ISSN: 2151-4658. DOI: 10.1002/acr.21606.

[13] Matthew R. Bong and Paul E. Di Cesare. “Stiffness After Total Knee Arthroplasty”. *JAAOS - Journal of the American Academy of Orthopaedic Surgeons* 12.3 (June 2004), p. 164. ISSN: 1067-151X. https://journals.lww.com/jaaos/fulltext/2004/05000/stiffness_after_total_knee_arthroplasty.4.aspx.

[14] Erik Zachwieja et al. “Manipulation Under Anesthesia and Stiffness After Total Knee Arthroplasty”. *JBJS Reviews* 6.4 (Apr. 2018), e2. ISSN: 2329-9185. DOI: 10.2106/JBJS.RVW.17.00113.

[15] HS Kan et al. *Non-surgical treatment of knee osteoarthritis*. Apr. 2019. https://www.hkmj.org/abstracts/v25n2/127.htm.

[16] R. R. Bannuru et al. “OARSI guidelines for the non-surgical management of knee, hip, and polyarticular osteoarthritis”. *Osteoarthritis and Cartilage* 27.11 (Nov. 2019), pp. 1578–1589. ISSN: 1063-4584. DOI: 10.1016/j.joca.2019.06.011.

[17] Shahnawaz Anwer and Ahmad Alghadir. “Effect of Isometric Quadriceps Exercise on Muscle Strength, Pain, and Function in Patients with Knee Osteoarthritis: A Randomized Controlled Study”. *Journal of Physical Therapy Science* 26.5 (May 2014), pp. 745–748. ISSN: 0915-5287. DOI: 10.1589/jpts.26.745.

[18] P Conaghan. “Update on osteoarthritis part 1: current concepts and the relation to exercise”. *British Journal of Sports Medicine* 36.5 (Oct. 2002), pp. 330–333. ISSN: 0306-3674. DOI: 10.1136/bjsm.36.5.330.

[19] Kathleen Kline Mangione et al. “The Effects of High-Intensity and Low-Intensity Cycle Ergometry in Older Adults With Knee Osteoarthritis”. *The Journals of Gerontology: Series A* 54.4 (Apr. 1999), pp. M184–M190. ISSN: 1079-5006. DOI: 10.1093/gerona/54.4.M184.

[20] Fangbo Bing et al. *Effects of cycling rehabilitation training on patients with knee osteoarthritis: A systematic review and meta□analysis*. ISSN: 2693-5015. Jan. 2023. DOI: 10.21203/rs.3.rs-2425616/v1.

[21] Barbara A. Springer. “Ride 2 Recovery’s Project HERO: Using cycling as part of rehabilitation”. *Physical Therapy in Sport* 14.2 (May 2013), pp. 77–86. ISSN: 1466-853X. DOI: 10.1016/j.ptsp.2012.11.001.

[22] Ines Kutzner et al. “Loading of the Knee Joint During Ergometer Cycling: Telemetric In Vivo Data”. *Journal of Orthopaedic & Sports Physical Therapy* 42.12 (Dec. 2012), pp. 1032–1038. ISSN: 0190-6011, 1938-1344. DOI: 10.2519/jospt.2012.4001.

[23] Ying Fang et al. “Effects of Workloads and Cadences on Frontal Plane Knee Biomechanics in Cycling”. *Medicine & Science in Sports & Exercise* 48.2 (Feb. 2016), p. 260. ISSN: 0195-9131. DOI: 10.1249/MSS.0000000000000759.

[24] Grace H. Lo et al. “Bicycling over a Lifetime Is Associated with Less Symptomatic Knee Osteoarthritis: Data from the Osteoarthritis Initiative”. *Medicine & Science in Sports & Exercise* 56.9 (Sept. 2024), p. 1678. ISSN: 0195-9131. DOI: 10.1249/MSS.0000000000003449.

[25] P. Oja et al. “Health benefits of cycling: a systematic review”. *Scandinavian Journal of Medicine & Science in Sports* 21.4 (2011), pp. 496–509. ISSN: 1600-0838. DOI: 10.1111/j.1600-0838.2011.01299.x.

[26] Fred de Laat et al. “Overcoming barriers to cycling for knee disarticulation and transfemoral prosthesis users: A pilot study in the Netherlands”. *Canadian Prosthetics & Orthotics Journal* 7 (Dec. 2024). DOI: 10.33137/cpoj.v7i2.44191.

[27] Claire B. Crossley et al. “A calibrated EMG-informed neuromusculoskeletal model can estimate hip and knee joint contact forces in cycling better than static optimisation”. *Journal of Biomechanics* (Feb. 2025), p. 112586. ISSN: 0021-9290. DOI: 10.1016/j.jbiomech.2025.112586.

[28] Rachel L. Thompson et al. “Lower-limb joint reaction forces and moments during modified cycling in healthy controls and individuals with knee osteoarthritis”. *Clinical Biomechanics* 71 (Jan. 2020), pp. 167–175. ISSN: 0268-0033. DOI: 10.1016/j.clinbiomech.2019.11.004.

[29] Charalambos Panayiotou Charalambous. “Knee Biomechanics: Tibiofemoral Articulation”. *The Knee Made Easy*. Ed. by Charalambos Panayiotou Charalambous. Cham: Springer International Publishing, 2022, pp. 59–102. ISBN: 978-3-030-54506-2. DOI: 10.1007/978-3-030-54506-2_3.

[30] Bernd J. Stetter et al. “Estimation of Knee Joint Forces in Sport Movements Using Wearable Sensors and Machine Learning”. *Sensors* 19.17 (Jan. 2019). Number: 17 Publisher: Multidisciplinary Digital Publishing Institute, p. 3690. ISSN: 1424-8220. DOI: 10.3390/s19173690.

[31] Rohan Kothurkar, Ramesh Lekurwale, and Mayuri Gad. “Comparison of Methods for Predicting Muscle Activations and Knee Joint Contact Forces During Squatting Using OpenSim”. *Proceedings of International Conference on Intelligent Manufacturing and Automation*. Ed. by Hari Vasudevan, Vijaya Kumar N. Kottur, and Amool A. Raina. Singapore: Springer Nature, 2023, pp. 533–540. ISBN: 978-981-19797-1-2. DOI: 10.1007/978-981-19-7971-2_51.

[32] Benjamin J. Fregly et al. “Grand challenge competition to predict in vivo knee loads”. *Journal of Orthopaedic Research* 30.4 (2012), pp. 503–513. ISSN: 1554-527X. DOI: 10.1002/jor.22023.

[33] Giorgio Cassiolas et al. “Knee Joint Contact Forces during High-Risk Dynamic Tasks: 90° Change of Direction and Deceleration Movements”. *Bioengineering* 10.2 (Feb. 2023). Number: 2 Publisher: Multidisciplinary Digital Publishing Institute, p. 179. ISSN: 2306-5354. DOI: 10.3390/bioengineering10020179.

[34] R.R Neptune and S.A Kautz. “Knee joint loading in forward versus backward pedaling: implications for rehabilitation strategies”. *Clinical Biomechanics* 15.7 (Aug. 2000), pp. 528–535. ISSN: 02680033. DOI: 10.1016/S0268-0033(00)00005-X.

[35] Rodrigo R. Bini and Thiago Ayala Di Alencar. “Non-traumatic Injuries in Cycling”. *Biomechanics of Cycling*. Ed. by Rodrigo R. Bini and Felipe P. Carpes. Cham: Springer International Publishing, 2014, pp. 55–62. ISBN: 978-3-319-05539-8. DOI: 10.1007/978-3-319-05539-8_6.

[36] Darryl D. D’Lima et al. “The Mark Coventry Award: In Vivo Knee Forces During Recreation and Exercise After Knee Arthroplasty”. *Clinical Orthopaedics and Related Research* 466.11 (Nov. 2008), pp. 2605–2611. ISSN: 1528-1132. DOI: 10.1007/s11999-008-0345-x.

[37] Haeun Yum et al. “Cycling kinematics in healthy adults for musculoskeletal rehabilitation guidance”. *BMC Musculoskeletal Disorders* 22.1 (Dec. 2021), p. 1044. ISSN: 1471-2474. DOI: 10.1186/s12891-021-04905-2.

[38] Rodrigo R. Bini and Patria A. Hume. “Effects of workload and pedalling cadence on knee forces in competitive cyclists”. *Sports Biomechanics* 12.2 (June 2013), pp. 93–107. ISSN: 1476-3141, 1752-6116. DOI: 10.1080/14763141.2012.731428.

[39] Kai-Han Liang et al. “A Clipless Pedal-Sensor System for Three Dimensional Kinetic Analysis During Cycling”. *Journal of Medical and Biological Engineering* 40.6 (Dec. 2020), pp. 917–922. ISSN: 1609-0985, 2199-4757. DOI: 10.1007/s40846-020-00572-1.

[40] Raoul Reiser, Jeffrey Broker, and Michael Peterson. “Knee Loads in the Standard and Recumbent Cycling Positions”. *Biomedical sciences instrumentation* 40 (Feb. 2004), pp. 36–42. https://www.researchgate.net/publication/8571773_Knee_Loads_in_the_Standard_and_Recumbent_Cycling_Positions.

[41] Rodrigo R Bini. “Patellofemoral and tibiofemoral forces in cyclists and triathletes: effects of saddle height”. 1 (2012). https://www.jsc-journal.com/index.php/JSC/article/view/4.

[42] Mats O. Ericson and Ralph Nisell. “Tibiofemoral joint forces during ergometer cycling”. *The American Journal of Sports Medicine* 14.4 (July 1986), pp. 285–290. ISSN: 0363-5465, 1552-3365. DOI: 10.1177/036354658601400407.

[43] Mathieu Menard et al. “Influence of saddle setback on knee joint forces in cycling”. *Sports Biomechanics* 19.2 (Mar. 2020), pp. 245–257. ISSN: 1476-3141, 1752-6116. DOI: 10.1080/14763141.2018.1466906.

[44] Rodrigo Bini. “Influence of saddle height in 3D knee loads commuter cyclists: A statistical parametric mapping analysis”. *Journal of Sports Sciences* 39.3 (Feb. 2021), pp. 275–288. ISSN: 0264-0414, 1466-447X. DOI: 10.1080/02640414.2020.1816289.

[45] Peter Kozlovič, Nejc Šarabon, and Borut Fonda. “3D Knee Loading during Stationary Cycling: A Comprehensive Model Development and Reliability Analysis”. *Applied Sciences* 11.2 (Jan. 2021), p. 528. ISSN: 2076-3417. DOI: 10.3390/app11020528.

[46] Rodrigo Bini and Patria Hume. “Reproducibility of lower limb motion and forces during stationary submaximal pedalling using wearable motion tracking sensors”. *Sports Biomechanics* 22.8 (Aug. 2023), pp. 1041–1062. ISSN: 1476-3141, 1752-6116. DOI: 10.1080/14763141.2020.1776760.

[47] Caitlin E. Clancy et al. “Muscle-driven simulations and experimental data of cycling”. *Scientific Reports* 13.1 (Dec. 2023), p. 21534. ISSN: 2045-2322. DOI: 10.1038/s41598-023-47945-5.

[48] Rodrigo Rico Bini et al. “Effects of moving forward or backward on the saddle on knee joint forces during cycling”. *Physical Therapy in Sport* 14.1 (Feb. 2013), pp. 23–27. ISSN: 1466853X. DOI: 10.1016/j.ptsp.2012.02.003.

[49] G Bergmann et al. “Hip contact forces and gait patterns from routine activities”. *Journal of Biomechanics* 34.7 (July 2001), pp. 859–871. ISSN: 0021-9290. DOI: 10.1016/S0021-9290(01)00040-9.

[50] Philipp Damm et al. “In vivo hip joint loads during three methods of walking with forearm crutches”. *Clinical Biomechanics* 28.5 (June 2013), pp. 530–535. ISSN: 0268-0033. DOI: 10.1016/j.clinbiomech.2012.12.003.

[51] Darryl D. D'Lima et al. "Tibial Forces Measured In Vivo After Total Knee Arthroplasty". *The Journal of Arthroplasty* 21.2 (Feb. 2006), pp. 255–262. ISSN: 0883-5403. DOI: 10.1016/j.arth.2005.07.011.

[52] I. Kutzner et al. "Loading of the knee joint during activities of daily living measured *in vivo* in five subjects". *Journal of Biomechanics* 43.11 (Aug. 2010), pp. 2164–2173. ISSN: 0021-9290. DOI: 10.1016/j.jbiomech.2010.03.046.

[53] Scott L. Delp et al. "OpenSim: Open-Source Software to Create and Analyze Dynamic Simulations of Movement". *IEEE Transactions on Biomedical Engineering* 54.11 (Nov. 2007). Conference Name: IEEE Transactions on Biomedical Engineering, pp. 1940–1950. ISSN: 1558-2531. DOI: 10.1109/TBME.2007.901024.

[54] Kieran J. Bennett et al. "EMG-Informed Neuromusculoskeletal Models Accurately Predict Knee Loading Measured Using Instrumented Implants". *IEEE Transactions on Biomedical Engineering* 69.7 (July 2022). Conference Name: IEEE Transactions on Biomedical Engineering, pp. 2268–2275. ISSN: 1558-2531. DOI: 10.1109/TBME.2022.3141067.

[55] Apoorva Rajagopal et al. "Full-Body Musculoskeletal Model for Muscle-Driven Simulation of Human Gait". *IEEE Transactions on Biomedical Engineering* 63.10 (Oct. 2016). Conference Name: IEEE Transactions on Biomedical Engineering, pp. 2068–2079. ISSN: 1558-2531. DOI: 10.1109/TBME.2016.2586891.

[56] Zachary F. Lerner et al. "How tibiofemoral alignment and contact locations affect predictions of medial and lateral tibiofemoral contact forces". *Journal of Biomechanics* 48.4 (Feb. 2015), pp. 644–650. ISSN: 0021-9290. DOI: 10.1016/j.jbiomech.2014.12.049.

[57] S.L. Delp et al. "An interactive graphics-based model of the lower extremity to study orthopaedic surgical procedures". *IEEE Transactions on Biomedical Engineering* 37.8 (Aug. 1990). Conference Name: IEEE Transactions on Biomedical Engineering, pp. 757–767. ISSN: 1558-2531. DOI: 10.1109/10.102791.

[58] Adrian K. M. Lai et al. "Lower-limb muscle function is influenced by changing mechanical demands in cycling". *Journal of Experimental Biology* 224.3 (Feb. 2021), jeb228221. ISSN: 0022-0949. DOI: 10.1242/jeb.228221.

[59] Bruno Luiz Souza Bedo et al. "A custom musculoskeletal model for estimation of medial and lateral tibiofemoral contact forces during tasks with high knee and hip flexions". *Computer Methods in Biomechanics and Biomedical Engineering* 23.10 (July 2020). Publisher: Taylor & Francis, pp. 658–663. ISSN: 1025-5842. DOI: 10.1080/10255842.2020.1757662.

[60] Scott D. Uhlrich et al. "Muscle coordination retraining inspired by musculoskeletal simulations reduces knee contact force". *Scientific Reports* 12.1 (July 2022). Publisher: Nature Publishing Group, p. 9842. ISSN: 2045-2322. DOI: 10.1038/s41598-022-13386-9.

[61] Alexandre R. M. Pelegrinelli et al. "Comparing three generic musculoskeletal models to estimate the tibiofemoral reaction forces during gait and sit-to-stand tasks". *Medical Engineering & Physics* 122 (Dec. 2023), p. 104074. ISSN: 1350-4533. DOI: 10.1016/j.medengphy.2023.104074.

[62] Anthony A. Gatti et al. "Hip and ankle kinematics are the most important predictors of knee joint loading during bicycling". *Journal of Science and Medicine in Sport* 24.1 (Jan. 2021), pp. 98–104. ISSN: 1440-2440. DOI: 10.1016/j.jsams.2020.07.001.

[63] Anthony A. Gatti et al. "Equations to Prescribe Bicycle Saddle Height based on Desired Joint Kinematics and Bicycle Geometry". *European Journal of Sport Science* 22.3 (2022), pp. 344–353. ISSN: 1536-7290. DOI: 10.1080/17461391.2021.1902570.

[64] Adam Trepczynski et al. "Impact of antagonistic muscle co-contraction on in vivo knee contact forces". *Journal of NeuroEngineering and Rehabilitation* 15.1 (Nov. 2018), p. 101. ISSN: 1743-0003. DOI: 10.1186/s12984-018-0434-3.

[65] M. Jorge and M. L. Hull. "Analysis of EMG measurements during bicycle pedalling". *Journal of Biomechanics* 19.9 (Jan. 1986), pp. 683–694. ISSN: 0021-9290. DOI: 10.1016/0021-9290(86)90192-2.

[66] D. T. Felson. "Osteoarthritis as a disease of mechanics". *Osteoarthritis and Cartilage* 21.1 (Jan. 2013), pp. 10–15. ISSN: 1063-4584. DOI: 10.1016/j.joca.2012.09.012.

[67] Jennifer L. Hicks et al. “Is My Model Good Enough? Best Practices for Verification and Validation of Musculoskeletal Models and Simulations of Movement”. *Journal of Biomechanical Engineering* 137.020905 (Feb. 2015). ISSN: 0148-0731. DOI: 10.1115/1.4029304.

[68] Richard Baker et al. “The Conventional Gait Model : The Success and Limitations”. May 2017, pp. 1–19. ISBN: 978-3-319-30808-1. DOI: 10.1007/978-3-319-30808-1_25-2.

[69] M. Fonseca et al. “The Conventional Gait Model’s sensitivity to lower-limb marker placement”. *Scientific Reports* 12.1 (Aug. 2022). Publisher: Nature Publishing Group, p. 14207. ISSN: 2045-2322. DOI: 10.1038/s41598-022-18546-5.

[70] Paul William Macdermid and Andrew M. Edwards. “Influence of crank length on cycle ergometry performance of well-trained female cross-country mountain bike athletes”. *European Journal of Applied Physiology* 108.1 (Jan. 2010), pp. 177–182. ISSN: 1439-6327. DOI: 10.1007/s00421-009-1197-0.

[71] J. C. Holmes, A. L. Pruitt, and N. J. Whalen. “Lower extremity overuse in bicycling”. *Clinics in Sports Medicine* 13.1 (Jan. 1994), pp. 187–205. ISSN: 0278-5919. https://pubmed-ncbi-nlm-nih-gov.tudelft.idm.oclc.org/8111852/.

[72] K. de Vey Mestdagh. “Personal perspective: in search of an optimum cycling posture”. *Applied Ergonomics* 29.5 (Oct. 1998), pp. 325–334. ISSN: 0003-6870. https://www-sciencedirect-com.tudelft.idm.oclc.org/science/article/pii/S000368709700080X.

[73] Will W. Peveler. “Effects of Saddle Height on Economy in Cycling”. *The Journal of Strength & Conditioning Research* 22.4 (July 2008), p. 1355. ISSN: 1064-8011. DOI: 10.1519/JSC.0b013e318173dac6.

[74] *Correct Cycling Posture When Riding the NEO Bike Series Trainer | Garmin Customer Support*. https://support.garmin.com/en-US/?faq=ezGb66xcnL3aWFzFG1fb66.

[75] *Discover Cometa’s emg systems*. https://www.cometasystems.com/.

[76] Hermie J Hermens et al. “Development of recommendations for SEMG sensors and sensor placement procedures”. *Journal of Electromyography and Kinesiology* 10.5 (Oct. 2000), pp. 361–374. ISSN: 1050-6411. DOI: 10.1016/S1050-6411(00)00027-4.

[77] Christine C. Raasch et al. “Muscle coordination of maximum-speed pedaling”. *Journal of Biomechanics* 30.6 (June 1997), pp. 595–602. ISSN: 0021-9290. DOI: 10.1016/S0021-9290(96)00188-1.

[78] Seyyed Arash Haghpanah et al. “Musculoskeletal Modeling and Control of the Lower Limb in Cycling Using an Optimal Central Pattern Generator”. *Iranian Journal of Science and Technology, Transactions of Mechanical Engineering* 47.3 (Sept. 2023), pp. 1121–1130. ISSN: 2364-1835. DOI: 10.1007/s40997-022-00566-1.

[79] Garmin and Garmin Ltd or its subsidiaries. *Garmin Connect™ Mobile*. https://www.garmin.com/nl-NL/p/125677/.

[80] Adrian K. M. Lai, Allison S. Arnold, and James M. Wakeling. “Why are Antagonist Muscles Co-activated in My Simulation? A Musculoskeletal Model for Analysing Human Locomotor Tasks”. *Annals of Biomedical Engineering* 45.12 (Dec. 2017), pp. 2762–2774. ISSN: 1573-9686. DOI: 10.1007/s10439-017-1920-7.

[81] Chisom Wilson and Tamara Bush. “Interface forces on the seat during a cycling activity”. *Clinical biomechanics (Bristol, Avon)* 22 (Dec. 2007), pp. 1017–23. DOI: 10.1016/j.clinbiomech.2007.06.004.

[82] Steven J. Elmer et al. “Joint-Specific Power Production during Submaximal and Maximal Cycling”. *Medicine & Science in Sports & Exercise* 43.10 (Oct. 2011), p. 1940. ISSN: 0195-9131. DOI: 10.1249/MSS.0b013e31821b00c5.

[83] Andrew R. Chapman et al. “The influence of body position on leg kinematics and muscle recruitment during cycling”. *Journal of Science and Medicine in Sport* 11.6 (Nov. 2008), pp. 519–526. ISSN: 1440-2440. DOI: 10.1016/j.jsams.2007.04.010.

[84] Nicolas A. Turpin and Bruno Watier. “Cycling Biomechanics and Its Relationship to Performance”. *Applied Sciences* 10.12 (Jan. 2020). Number: 12 Publisher: Multidisciplinary Digital Publishing Institute, p. 4112. ISSN: 2076-3417. DOI: 10.3390/app10124112.

[85] Janelle M. Kaneda et al. “Can static optimization detect changes in peak medial knee contact forces induced by gait modifications?” *Journal of Biomechanics* 152 (May 2023), p. 111569. ISSN: 0021-9290. DOI: 10.1016/j.jbiomech.2023.111569.

[86] Tishya A. L. Wren et al. “Cross-correlation as a method for comparing dynamic electromyography signals during gait”. *Journal of Biomechanics* 39.14 (Jan. 2006), pp. 2714–2718. ISSN: 0021-9290. DOI: 10.1016/j.jbiomech.2005.09.006.

[87] Katherine M. Steele et al. “Compressive Tibiofemoral Force during Crouch Gait”. *Gait & posture* 35.4 (Apr. 2012), pp. 556–560. ISSN: 0966-6362. DOI: 10.1016/j.gaitpost.2011.11.023.

[88] Italo Belli et al. “Does enforcing glenohumeral joint stability matter? A new rapid muscle redundancy solver highlights the importance of non-superficial shoulder muscles”. *PLOS ONE* 18.11 (Nov. 2023), e0295003. ISSN: 1932-6203. DOI: 10.1371/journal.pone.0295003.

[89] Andrew Horwood and Nachiappan Chockalingam. “Chapter 4 - Internal force generation”. *Clinical Biomechanics in Human Locomotion*. Ed. by Andrew Horwood and Nachiappan Chockalingam. Academic Press, Jan. 2023, pp. 315–390. ISBN: 978-0-323-85212-8. DOI: 10.1016/B978-0-323-85212-8.00004-3.

[90] Felix E Zajac. “Understanding muscle coordination of the human leg with dynamical simulations”. *Journal of Biomechanics* 35.8 (Aug. 2002), pp. 1011–1018. ISSN: 0021-9290. DOI: 10.1016/S0021-9290(02)00046-5.

[91] Anthony A. Gatti et al. “Acute changes in knee cartilage transverse relaxation time after running and bicycling”. *Journal of Biomechanics* 53 (Feb. 2017), pp. 171–177. ISSN: 0021-9290. DOI: 10.1016/j.jbiomech.2017.01.017.

[92] Florian Michaud et al. *Influence of muscle recruitment criteria on joint reaction forces during human gait*. June 2015. https://www.researchgate.net/publication/318701201_Influence_of_muscle_recruitment_criteria_on_joint_reaction_forces_during_human_gait.

[93] Gerrit Jan van Ingen Schenau, Carol A. Pratt, and Jane M. Macpherson. “Differential use and control of mono- and biarticular muscles”. *Human Movement Science* 13.3 (Aug. 1994), pp. 495–517. ISSN: 0167-9457. DOI: 10.1016/0167-9457(94)90051-5.

[94] Rodrigo Bini, Felipe Carpes, and Fernando Diefenthaeler. “Effects of cycling with the knees close to the bicycle frame on the lower limb muscle activation”. *Revista Brasileira de Educação Física e Esporte* 25 (Mar. 2011), pp. 27–37. DOI: 10.1590/S1807-55092011000100004.

[95] Rodrigo R. Bini and Felipe P. Carpes, eds. *Biomechanics of Cycling*. Cham: Springer International Publishing, 2014. ISBN: 978-3-319-05538-1 978-3-319-05539-8. DOI: 10.1007/978-3-319-05539-8.

[96] Sangsoo Park and Graham E. Caldwell. “Muscular activity patterns in 1-legged *vs.* 2-legged pedaling”. *Journal of Sport and Health Science* 10.1 (Jan. 2021), pp. 99–106. ISSN: 2095-2546. DOI: 10.1016/j.jshs.2020.01.003.

[97] Julio Cézar Lima da Silva et al. “Quadriceps and hamstring muscle activity during cycling as measured with intramuscular electromyography”. *European Journal of Applied Physiology* 116 (2016), pp. 1807–1817. ISSN: 1439-6319. DOI: 10.1007/s00421-016-3428-5.

[98] Marion Crouzier et al. “Neuromechanical coupling within the human triceps surae and its consequence on individual force-sharing strategies”. *Journal of Experimental Biology* 221.21 (Nov. 2018), jeb187260. ISSN: 0022-0949. DOI: 10.1242/jeb.187260.

[99] Sangsoo Park, Graham E. Caldwell, and Brian R. Umberger. “A direct collocation framework for optimal control simulation of pedaling using OpenSim”. *PLoS ONE* 17.2 (Feb. 2022), e0264346. DOI: 10.1371/journal.pone.0264346.

[100] W. Herzog, D. Longino, and A. Clark. “The role of muscles in joint adaptation and degeneration”. *Langenbeck’s Archives of Surgery* 388.5 (Oct. 2003), pp. 305–315. ISSN: 1435-2451. DOI: 10.1007/s00423-003-0402-6.

[101] Adam Trepczynski et al. “Modulation of the Relationship Between External Knee Adduction Moments and Medial Joint Contact Forces Across Subjects and Activities”. *Arthritis & Rheumatology* 66.5 (2014), pp. 1218–1227. ISSN: 2326-5205. DOI: 10.1002/art.38374.

[102] Matthew S. DeMers, Saikat Pal, and Scott L. Delp. “Changes in Tibiofemoral Forces due to Variations in Muscle Activity during Walking”. *Journal of orthopaedic research : official publication of the Orthopaedic Research Society* 32.6 (Feb. 2014), p. 769. DOI: 10.1002/jor.22601.

[103] S. Dorel, A. Couturier, and F. Hug. “Influence of different racing positions on mechanical and electromyographic patterns during pedalling”. *Scandinavian Journal of Medicine & Science in Sports* 19.1 (2009), pp. 44–54. ISSN: 1600-0838. DOI: 10.1111/j.1600-0838.2007.00765.x.

[104] Ines Kutzner et al. “Knee Adduction Moment and Medial Contact Force – Facts about Their Correlation during Gait”. *PLoS ONE* 8.12 (Dec. 2013), e81036. ISSN: 1932-6203. DOI: 10.1371/journal.pone.0081036.

[105] Jana Holder et al. “Peak knee joint moments accurately predict medial and lateral knee contact forces in patients with valgus malalignment”. *Scientific Reports* 13.1 (Feb. 2023). Publisher: Nature Publishing Group, p. 2870. ISSN: 2045-2322. DOI: 10.1038/s41598-023-30058-4.

[106] W. F. van de Meerakker. “Development of an MRI-based Automatic Segmentation Model to analyze Sex-Related Differences in the Lower-extremity Musculoskeletal System” (2025). https://repository.tudelft.nl/record/uuid:c7b8ad57-e4db-49ae-ae0f-049608c630be.

[107] Justin Fernandez et al. “A Narrative Review of Personalized Musculoskeletal Modeling Using the Physiome and Musculoskeletal Atlas Projects” (Aug. 2023). Section: Journal of Applied Biomechanics. ISSN: 2023-0079. https://journals.humankinetics.com/view/journals/jab/39/5/article-p304.xml.

[108] Massoud Akbarshahi et al. “Non-invasive assessment of soft-tissue artifact and its effect on knee joint kinematics during functional activity”. *Journal of Biomechanics* 43.7 (May 2010), pp. 1292–1301. ISSN: 0021-9290. DOI: 10.1016/j.jbiomech.2010.01.002.

[109] Tsung-Yuan Tsai et al. “Effects of soft tissue artifacts on the calculated kinematics and kinetics of the knee during stair-ascent”. *Journal of Biomechanics* 44.6 (Apr. 2011), pp. 1182–1188. ISSN: 0021-9290. DOI: 10.1016/j.jbiomech.2011.01.009.

[110] Ann-Kathrin Einfeldt et al. “A new method called MiKneeSoTA to minimize knee soft-tissue artifacts in kinematic analysis”. *Scientific Reports* 14.1 (Sept. 2024). Publisher: Nature Publishing Group, p. 20666. ISSN: 2045-2322. DOI: 10.1038/s41598-024-71409-z.

[111] L. M. S. Damink. “The comparison of skin mounted versus virtual ASIS markers in pelvic kinematics during gait, considering the effects of obesity” (2025). https://repository.tudelft.nl/record/uuid:c278425f-8cc6-4ea1-9370-7e070824a460.

[112] Sabrina Hörmann et al. “Development and validation of a 3DOF ellipsoidal bi-condylar knee joint for musculoskeletal modeling”. *International Symposium on Computer Simulation in Biomechanics* (July 2025).

[113] Scott K. Lynn, Samantha M. Reid, and Patrick A. Costigan. “The influence of gait pattern on signs of knee osteoarthritis in older adults over a 5–11 year follow-up period: A case study analysis”. *The Knee* 14.1 (Jan. 2007), pp. 22–28. ISSN: 0968-0160. DOI: 10.1016/j.knee.2006.09.002.

[114] J. L. Astephen Wilson and D. Kobsar. “Osteoarthritis year in review 2020: mechanics”. *Osteoarthritis and Cartilage* 29.2 (Feb. 2021). Publisher: Elsevier, pp. 161–169. ISSN: 1063-4584, 1522-9653. DOI: 10.1016/j.joca.2020.12.009.

[115] Mel S. Lee et al. “Effects of shear stress on nitric oxide and matrix protein gene expression in human osteoarthritic chondrocytes in vitro”. *Journal of Orthopaedic Research* 20.3 (2002), pp. 556–561. ISSN: 1554-527X. DOI: 10.1016/S0736-0266(01)00149-8.

[116] Mel S. Lee et al. “Regulation of nitric oxide and bcl-2 expression by shear stress in human osteoarthritic chondrocytes in vitro”. *Journal of Cellular Biochemistry* 90.1 (2003), pp. 80–86. ISSN: 1097-4644. DOI: 10.1002/jcb.10611.

[117] Christian Egloff, Thomas Hügle, and Victor Valderrabano. “Biomechanics and pathomechanisms of osteoarthritis”. *Swiss Medical Weekly* 142.2930 (July 2012). Number: 2930, w13583–w13583. ISSN: 1424-3997. DOI: 10.4414/smw.2012.13583.

[118] Annegret Mündermann, Chris O. Dyrby, and Thomas P. Andriacchi. “Secondary gait changes in patients with medial compartment knee osteoarthritis: Increased load at the ankle, knee, and hip during walking”. *Arthritis & Rheumatism* 52.9 (2005), pp. 2835–2844. ISSN: 1529-0131. DOI: 10.1002/art.21262.

[119] Ventura Ferrer-Roca et al. “Acute effects of small changes in crank length on gross efficiency and pedalling technique during submaximal cycling”. *Journal of Sports Sciences* 35.14 (July 2017). Publisher: Routledge, pp. 1328–1335. ISSN: 0264-0414. DOI: 10.1080/02640414.2016.1215490.

[120] Darryl G. Thelen, Frank C. Anderson, and Scott L. Delp. “Generating dynamic simulations of movement using computed muscle control”. *Journal of Biomechanics* 36.3 (Mar. 2003), pp. 321–328. ISSN: 0021-9290. DOI: 10.1016/S0021-9290(02)00432-3.

[121] Hoa X. Hoang et al. “A calibrated EMG-informed neuromusculoskeletal model can appropriately account for muscle co-contraction in the estimation of hip joint contact forces in people with hip osteoarthritis”. *Journal of Biomechanics* 83 (Jan. 2019), pp. 134–142. ISSN: 0021-9290. DOI: 10.1016/j.jbiomech.2018.11.042.

[122] Taylor J. M. Dick et al. “Consensus for experimental design in electromyography (CEDE) project: Application of EMG to estimate muscle force”. *Journal of Electromyography and Kinesiology* 79 (Dec. 2024), p. 102910. ISSN: 1050-6411. DOI: 10.1016/j.jelekin.2024.102910.

[123] Reza Ahmadi et al. “A Machine Learning Approach for Predicting Pedaling Force Profile in Cycling”. *Sensors (Basel, Switzerland)* 24.19 (Oct. 2024), p. 6440. DOI: 10.3390/s24196440.

[124] Scott D. Uhlrich et al. *OpenCap: 3D human movement dynamics from smartphone videos*. Pages: 2022.07.07.499061 Section: New Results. July 2022. DOI: 10.1101/2022.07.07.499061.

[125] Niels Dur et al. “Fluoroscopy: Taking a closer look at joint motion in osteoarthritis”. *Osteoarthritis Imaging* 4.3 (Sept. 2024). DOI: 10.1016/j.ostima.2024.100240.

[126] Vera Pinskerova and Pavel Vavrik. “Knee Anatomy and Biomechanics and its Relevance to Knee Replacement”. *Personalized Hip and Knee Joint Replacement*. Ed. by Charles Rivière and Pascal-André Vendittoli. Cham (CH): Springer, 2020. ISBN: 978-3-030-24242-8 978-3-030-24243-5. http://www.ncbi.nlm.nih.gov/books/NBK565765/.

[127] *Palpation*. https://pycgm2.netlify.app/ressources/palpation/.

[128] Kevin Deschamps et al. “Body of evidence supporting the clinical use of 3D multisegment foot models: A systematic review”. *Gait & Posture* 33.3 (Mar. 2011), pp. 338–349. ISSN: 09666362. DOI: 10.1016/j.gaitpost.2010.12.018.

A

Marker placement

The following section explains how optical motion capture markers were placed before the experiment, according to the CGM2.4 marker placement guidelines [127]. A total of 34 markers were placed [128]. This appendix does not elaborate on the positioning of the pedal markers.

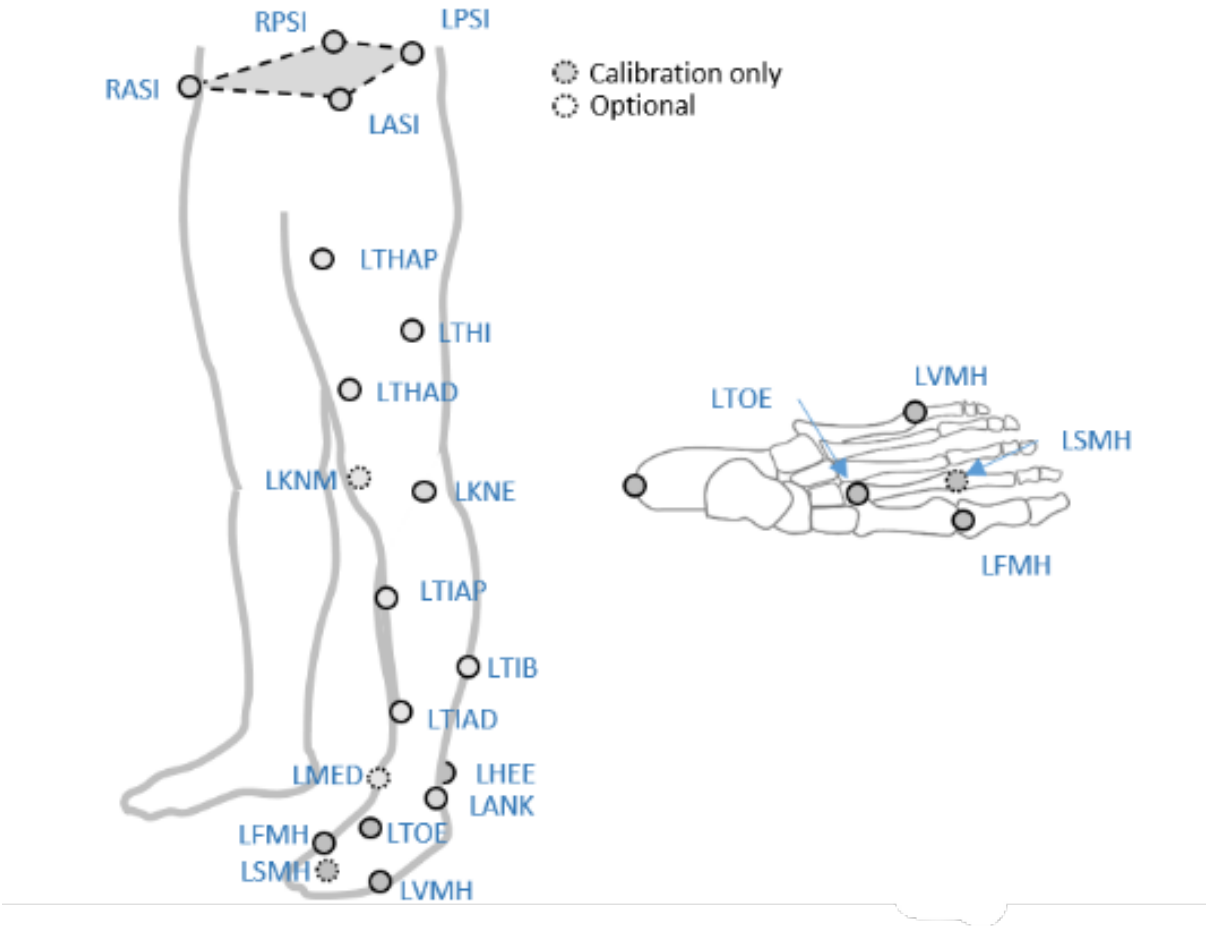

Figure A.1: Marker placement for standard CGM2.4 model [128].

Pelvis markers

Left and Right Posterior Superior Iliac Spine (LPSI, RPSI)

- Place the markers over the posterior superior iliac spine bilaterally.

Left and Right Anterior Superior Iliac Spine (LASI, RASI)

- Place the markers over the anterior superior iliac spine bilaterally.

Thigh markers

Left and Right Lateral Thigh (LTHI, RTHI)

- Place the markers halfway down the lateral thigh.
- Use the ASIS markers and the epicondyle markers to define the length of the femur.

Left and Right Thigh Anterior Proximal (LHTAP, RHTAP)

- Place the markers one-third down the anterior thigh.
- Use the ASIS markers and the epicondyle markers to define the length of the femur.

Left and Right Thigh Anterior Distal (LHTAD, RHTAD)

- Place the markers two-thirds down the anterior thigh.
- Use the ASIS markers and the epicondyle markers to define the length of the femur.

Knee markers

Left and Right Lateral Epicondyle (LKNE, RKNE)

- Place the markers over the most prominent aspect of the lateral epicondyle.

Left and Right Medial Epicondyle (LKNM, RKNM)

- Place the markers over the most prominent aspect of the medial epicondyle.

Tibia markers

Left and Right Lateral Lower Leg (LTIB, RTIB)

- Place the markers halfway down the lateral lower leg.
- Use the femoral epicondyle and malleoli markers to define the length of the tibia.

Left and Right Tibia Anterior Proximal (LTIAP, RTIAP)

- Place the marker 2 cm distal to the tibial tubercle.

Left and Right Tibia Anterior Distal (LTIAD, RTIAD)

- Halfway down the tibia’s crest.

Foot and Ankle markers

Left and Right Lateral Malleolus (LANK, RANK)

- Place the markers so that the distal tip of the baseplate lines up with the most distal aspect of the malleolus.

Left and Right Medial Malleolus (LMED, RMED)

- Place the markers so that the distal tip of the baseplate lines up with the most distal aspect of the malleolus.

Left and Right Heel (LHEE, RHEE)

- Place the top of the baseplate so that it is over the most prominent aspect of the posterior calcaneus.

Left and Right 2nd Metatarso-Cuneiform Joint (LTOE, RTOE)

- Place the middle of the marker over the metatarso-cuneiform joint in the center of the metatarsal.

Left and Right 5th Metatarsophalangeal Joint (LVMH, RVMH)

- Place the center of the baseplate on the line of the fifth metatarsophalangeal joint (dorsal aspect).

Left and Right 1st Metatarsophalangeal Joint (LFMH, RFMH)

- Place the markers at the first metatarsophalangeal joint on the dorsal aspect.

Left and Right 2nd Metatarsophalangeal Joint (LSMH, RSMH)

- Place the markers at the second metatarsophalangeal joint so that they are centered over the bone.

B

Marker based model adjustments

To ensure compatibility of our method with both the online dataset and our own experimental setup, two different marker models were implemented. One model replicates the marker positions used in the publicly available dataset from Gatti et al. [62, 63], while the other uses marker placements based on the Conventional Gait Model (CGM) (Appendix A), which aligns with our motion capture protocol using Nexus software.

Figure B.1 illustrates the difference between these two marker models. In each case, the model is shown after scaling (left) and after running Inverse Kinematics (right) with the right pedal at TDC. These visualizations highlight how the same musculoskeletal framework can be adapted to accommodate different marker configurations, ensuring consistency across data sources.

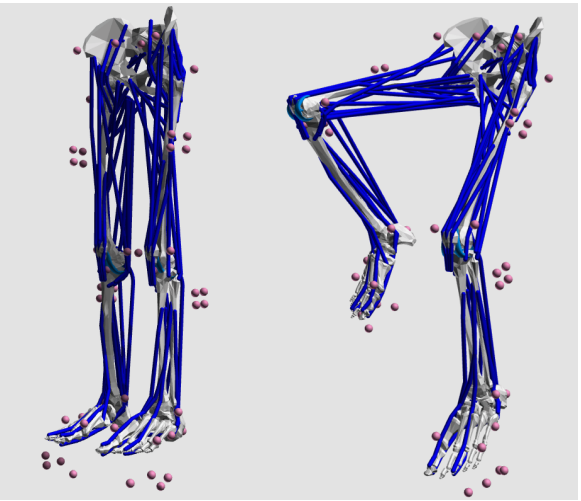

(a) The generic model using marker positions from Gatti et al. [62, 63]. Left: after scaling. Right: after Inverse Kinematics with right pedal on top dead centre (TDC).

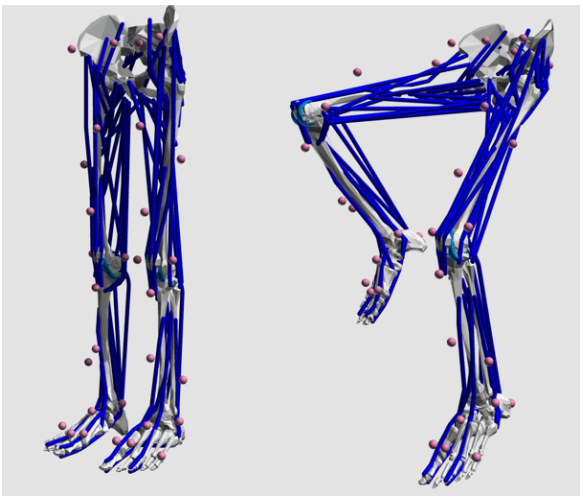

(b) The generic model using marker positions from the Conventional Gait Model (CGM). Left: after scaling. Right: after Inverse Kinematics with right pedal on top dead centre (TDC).

Figure B.1: Comparison of the generic models developed for this study. (a) shows the model based on Gatti et al., and (b) shows the model based on CGM2.4.

C

Participant data

C.1. All participants

Gatti et al. participants

Participant	Age (years)	Sex	Height (cm)	Weight (kg)	Cadence (RPM)	Power (W)
P01	29	Female	169.0	60.4	77	60
P02	22	Male	182.2	92.3	80	107
P03	21	Male	171.2	74.2	83	120
P04	23	Female	166.2	61.1	92	81
P05	28	Male	195.4	90.8	84	136
P06	27	Male	181.7	77.3	90	216
P07	41	Male	188.1	79.4	92	161
P08	42	Male	173.0	66.5	90	117
P09	26	Male	179.8	76.1	75	156
P10	19	Male	183.5	89.3	85	160
P11	32	Female	163.1	54.2	78	94
P12	31	Male	183.7	91.5	80	116
P13	44	Male	191.6	83.0	90	199
P14	42	Female	159.8	56.7	86	40
P15	31	Female	168.5	57.1	85	144
P16	35	Male	179.6	78.0	89	208

Table C.1: Cycling and anthropometric data of participants from the dataset [62, 63] used by Clancy et al. [47].

MOBI lab participants

Participant	Age (years)	Sex	Height (cm)	Weight (kg)	Cycling / Week (h)	(km)	Knee Width (mm)	Ankle Width (mm)	Inseam Length (cm)
P01	25	Male	193.0	79.1	5	80	103.0	78.6	105.0
P02	28	Male	185.9	76.7	5	50	93.3	69.8	95.5
P03	25	Male	174.8	76.6	4	60	98.8	71.5	89.0
P04	30	Female	176.8	69.5	2	50	96.8	67.0	95.0
P05	24	Male	184.3	79.9	3.5	80	110.2	73.7	98.0
P06	25	Female	174.1	57.5	5	55	89.2	64.9	88.5
P07	25	Male	178.8	68.5	6	50	97.9	65.1	93.0
P08	26	Female	176.0	80.3	1.5	40	117.1	72.3	94.5
P09	25	Male	198.0	86.3	7	100	111.0	70.4	108.5
P10	25	Female	174.0	60.3	4	30	96.8	66.2	91.0
P11	25	Male	193.3	106.1	2	40	106.2	75.3	103.5

Table C.2: Cycling and anthropometric data of participants from the experiments in the MOBI laboratory.

C.2. Selected participants for comparison

Pair	Participant	1st TDC (15-25s)	Condition
Pair 1	MOBI06	15.45	80 RPM - 100 W
Pair 2	MOBI03	15.64	80 RPM - 120 W
Pair 3	MOBI10	15.21	90 RPM - 80 W
Pair 4	MOBI09	15.08	80 RPM - 120 W
Pair 5	MOBI07	15.22	90 RPM - 120 W

(a) Selected participants from the MOBI experiments, including the first detected Top Dead Centre (TDC) within the time frame of 15-25 seconds.

Pair	Participant	1st TDC (120-130s)	TDC after 10 cycles	Condition
Pair 1	Gatti P11	120.03	127.80	78 RPM - 94 W
Pair 2	Gatti P03	120.53	127.88	83 RPM - 120 W
Pair 3	Gatti P04	120.57	127.06	92 RPM - 81 W
Pair 4	Gatti P05	120.53	127.92	84 RPM - 136 W
Pair 5	Gatti P08	120.62	127.23	90 RPM - 117 W

(b) Selected participants from the online dataset of Gatti et al. [62, 63], including the first and the tenth detected Top Dead Centre (TDC) within the time frame of 120-130 seconds.

Table C.3: Selected participants, including the detected Top Dead Centre (TDC).

D

Development of the MOBI-cycling laboratory

To develop the hospital-based cycling laboratory, the following key hardware components were required:

1. A bike with adjustable saddle and handlebars, capable of measuring cadence and power output.
2. Instrumented pedals for measuring 3D forces and moments, with the ability to synchronise kinetic and kinematic data.
3. A motion capture system using retroreflective markers
4. Electromyography (EMG) sensors

Neo Tacx bike setup

A Neo Tacx Bike was borrowed from the Bicycle Lab at TU Delft. The saddle and handlebars were adjustable both horizontally and vertically. The crank arm length could also be adjusted, with fixed positions at 170 mm, 172.5 mm, or 175 mm.

The bike was positioned on the treadmill (Figure D.1), with its midline aligned along the laboratory's z-axis. Integrated fans responded dynamically to the power output during pedalling.

Connection to the Garmin Connect app [79] via Bluetooth allowed for control over resistance and gear settings, enabling fine-tuned power output adjustments.

Figure D.1: Cycling setup with the bike on the treadmill, and two motion capture cameras are mounted on tripods: one in front and one behind the bike

Instrumented pedals for pedal reaction force analysis

Interviews have been held with Sensix (Poitiers, France), on the possibility of using two instrumented pedals for measuring the pedal reaction force (PRF) during cycling. Unfortunately, these were not possible to arrange in the short term.

As an alternative, instrumented pedals from the University of Twente were tested (Figure D.2). These can be connected via analogue cables to the lab computer. Despite the proper setup, the force-torque sensors did not register any output when the load was applied. Consequently, this option was abandoned.

Ultimately, an attempt was made to estimate the PRF (Appendix H). However, this approach introduced additional complications, and PRF analysis was therefore excluded from the final scope of this study.

Figure D.2: Sandals with two force-torques sensors below the sole

Markers and motion capture system

The laboratory was already equipped with 12 motion capture cameras (VICON Vero, Oxford, United-Kingdom) and retroreflective markers. Ten cameras were fixed to the laboratory walls. Two additional cameras were mounted on tripods (see Figure D.1) and placed in front and behind the bike to improve visibility of medial ankle and knee markers, particularly near the Bottom Dead Centre (BDC), where occlusion was likely.

The motion capture was analysed using Nexus Software (v15.9).

EMG Cometa Mini45

Electromyography (EMG) sensors of Cometa (Mini45) were borrowed from the Gait Analysis Laboratory of the TU Delft. These sensors wirelessly transmitted signals to a Bluetooth amplifier, which was connected via an analogue signal interface box (Figure D.3a) and a Weidmüller connector (Figure D.3b) to the laboratory computer. The EMG voltage could be directly read out with the Nexus Software, including time-synchronisation with the kinematic motion capture data from Vicon.

(a) The analog signal interference box from Cometa.

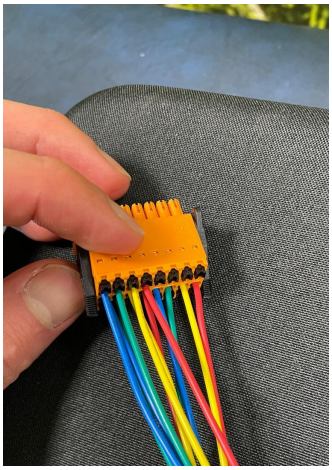

(b) The analog signals from the analog signal interference box into the Weidmüller connector (orange).

Figure D.3: Analog signal interference box and Weidmüller connector to analyse the EMG data.

E

Experimental protocol

This document describes the procedure each participant will follow during the experiment.

The aim of this study is to investigate medial and lateral knee loading during cycling by analysing knee joint contact forces under different conditions. Eleven healthy adult participants will participate in this study. The experiment will be conducted in the MOBI lab at the Erasmus Medical Centre, a motion capture lab established within the Convergence collaboration of TU Delft and Erasmus MC. TUD and EMC supervisors are actively involved in the lab and this experiment and collaborate closely on the project.

The project will be part of the LOAD project, a multidisciplinary collaboration involving, among others, TU Delft and Erasmus MC. The LOAD project focuses on determining what constitutes healthy stress for an individual with knee osteoarthritis and how patients can be guided to move healthy.

When participants arrive, they will be given an introduction to the study and have time to review, ask questions about, and sign the informed consent form. Next, small, lightweight motion capture markers will be placed on specific anatomical landmarks, such as the hip, thigh, and lower leg, to accurately track the motion of your joints during the activity, in alignment with the Conventional Gait Model (CGM) guidelines.

Additionally, seven electromyography (EMG) sensors will be attached to the skin of the right leg over the following muscles: The rectus femoris, vastus lateralis, vastus medialis, gastrocnemius lateralis, gastrocnemius medialis, biceps femoris, and semitendinosus.

These non-invasive sensors measure the electrical activity of muscles as they contract during cycling. Please note that some skin hair may need to be gently removed in the sensor areas to ensure proper contact and accurate readings. This setup enables precise data capture on joint movement and muscle performance, providing a detailed understanding of biomechanics during the activity.

Participants will perform a brief 2-minute warm-up at a self-chosen cadence and power output to familiarize themselves with the setup. The main cycling session will involve nine 30-seconds intervals, each at varying cadences between 70 and 90 RPM and power levels between 80 and 120 W, designed to simulate a range of typical cycling intensities without causing fatigue.

Data collected from the optical motion capture system will be integrated with a musculoskeletal model to calculate knee joint contact forces, offering insights into the distribution of loads across the medial and lateral compartments of the knee during cycling. The EMG data will be used for validation purposes of the model. To normalize the EMG data, the participants are instructed to perform 2 squat jumps and finish the measurements with a cycling sprint on the bike.

Lab preparation

1. Turn on the Vicon system
2. Relocate the bike to the correct position
3. Connect the bike to electricity

4. Connect the app with the bike via Bluetooth
5. Put a sheet over the research bench
6. Prepare a box with: 36 markers, tape, measuring tape, and an electronic caliper (schuifmaat), angle measurement device
7. Prepare a box with all the EMG equipment: shaving foam, shaver, tape, emg-sensors 1 to 8
8. Prepare the consent form with a pen
9. Remove everything that could be recognized as a marker
10. Calibrate the camera's
11. Define the ground/zero, by placing the wand on the treadmill

Participant

1. Pick up the participant from the entrance
2. Introduce Wouter
3. Explain briefly what you are going to do today
4. Change clothes (sport socks, tight sports/cycling shorts, sport shirt)
5. Show the participant the consent form and let him/her sign it
6. Measure the weight of the participant
7. Measure the height of the participant
8. Measure the ankle width
9. Measure the knee width
10. Measure the leg length
11. Set the saddle height so that the knee is in a 25-30 degree flexion angle
12. Set the handlebar at the same height as the saddle
13. Set the horizontal saddle position so that the patella is in line with the crank axis
14. Set the horizontal handlebar position so that the torso is at 90 degrees with the upper arms when the hands are on top of the handlebar
15. Remove the hairs and put alcohol on the skin where the EMG sensors will be placed
16. Place EMG sensors on the:
    a. Rectus Femoris
    b. Vastus Lateralis
    c. Vastus Medialis
    d. Gastrocnemius Lateralis
    e. Gastrocnemius Medialis
    f. Biceps Femoris
    g. Semitendinosus
    h. Reserve
17. Place the markers together with Wouter
18. Make a picture of the lower extremities with markers and EMG for postprocessing purposes

Static and dynamic trial

1. Place the participant behind the treadmill
2. Place the participant on the treadmill close to the bike
3. Perform a static trial behind the bike
4. Let the participant perform a squat jump to measure the maximum voluntary contraction of the participant

5. Perform a static trial *over* the bike
6. Perform a dynamic trial by getting on the bike and start cycling
7. Make sure the participant can move freely without cables being overthrown and markers falling off
8. Make a picture of the cycling position with all the markers and EMG for postprocessing purposes

Experiment

1. Make the participant warm up for 2 minutes on a self-chosen cadence
2. 30s of cycling on:
    - cadence = 70 RPM and power output = 80 W
3. 30s rest, switching conditions
4. 30s of cycling on:
    - cadence = 80 RPM and power output = 80 W
5. 30s rest, switching conditions
6. 30s of cycling on:
    - cadence = 90 RPM and power output = 80 W
7. 30s rest, switching conditions
8. 30s of cycling on:
    - cadence = 70 RPM and power output = 100 W
9. 30s rest, switching conditions
10. 30s of cycling on:
    - cadence = 80 RPM and power output = 100 W
11. 30s rest, switching conditions
12. 30s of cycling on:
    - cadence = 90 RPM and power output = 100 W
13. 30s rest, switching conditions
14. 30s of cycling on:
    - cadence = 70 RPM and power output = 120 W
15. 30s rest, switching conditions
16. 30s of cycling on:
    - cadence = 80 RPM and power output = 120 W
17. 30s rest, switching conditions
18. 30s of cycling on:
    - cadence = 90 RPM and power output = 120 W
19. 10s of rest switching the power output to 200W
20. 5s sprint on 200W and self-chosen cadence:
    - Cadence = self-chosen and power output = 200W
21. 30s of cooling down on a self-chosen cadence and power output
22. Total cycling time = 11.5 minutes

Round-up

1. Remove the bike from the treadmill
2. Calibrate the treadmill
3. Perform a slow squat on the treadmill
4. Perform a fast squat on the treadmill
5. Perform a jump squat on the treadmill
6. Remove the emg sensors and place them back in the box
7. Put the emg-sensors back in the charger
8. Remove the markers and place them back in a box
9. Save the consent form in a map with all the other consent forms
10. Save the data collection forms in a map with all the other data collection forms

F

Reserve actuator settings

Listing F.1: Reserve actuator settings file used for Static Optimisation with the Modified Model. This file is an expansion of the CMC actuator file of Rajagopal et al.

```
<?xml version="1.0" encoding="UTF-8"?>
<OpenSimDocument Version="30000">
    <ForceSet name="LowerBodyReserveActuators">
        <defaults>
            <CoordinateActuator name="default">
                <min_control>-Inf</min_control>
                <max_control>Inf</max_control>
                <coordinate></coordinate>
                <optimal_force>100</optimal_force>
            </CoordinateActuator>
        </defaults>
        <objects>
            <PointActuator name="FX">
                <body>pelvis</body>
                <point>-0.073 -0.02525 0</point>
                <direction>1 -0 -0</direction>
                <optimal_force>100</optimal_force>
                <min_control>-Inf</min_control>
                <max_control>Inf</max_control>
            </PointActuator>
            <PointActuator name="FY">
                <body>pelvis</body>
                <point>-0.073 -0.02525 0</point>
                <direction>-0 1 -0</direction>
                <optimal_force>100</optimal_force>
                <min_control>-Inf</min_control>
                <max_control>Inf</max_control>
            </PointActuator>
            <PointActuator name="FZ">
                <body>pelvis</body>
                <point>-0.073 -0.02525 0</point>
                <direction>-0 -0 1</direction>
                <optimal_force>100</optimal_force>
                <min_control>-Inf</min_control>
                <max_control>Inf</max_control>
            </PointActuator>
            <TorqueActuator name="MX">
                <bodyA>pelvis</bodyA>
                <bodyB>ground</bodyB>
                <axis>1 -0 -0</axis>
                <optimal_force>150</optimal_force>
                <min_control>-Inf</min_control>
                <max_control>Inf</max_control>
            </TorqueActuator>
            <TorqueActuator name="MY">
                <bodyA>pelvis</bodyA>
                <bodyB>ground</bodyB>
                <axis>-0 1 -0</axis>
                <optimal_force>150</optimal_force>
```

```
                <min_control>-Inf</min_control>
                <max_control>Inf</max_control>
            </TorqueActuator>
            <TorqueActuator name="MZ">
                <bodyA>pelvis</bodyA>
                <bodyB>ground</bodyB>
                <axis>-0 -0 1</axis>
                <optimal_force>150</optimal_force>
                <min_control>-Inf</min_control>
                <max_control>Inf</max_control>
            </TorqueActuator>
% ------------ (Coordinate Actuators Start Here) ------------
            <CoordinateActuator name="hip_flexion_r_reserve">
                <min_control>-Inf</min_control>
                <max_control>Inf</max_control>
                <coordinate>hip_flexion_r</coordinate>
                <optimal_force>2.5</optimal_force>
            </CoordinateActuator>
            <CoordinateActuator name="hip_adduction_r_reserve">
                <min_control>-Inf</min_control>
                <max_control>Inf</max_control>
                <coordinate>hip_adduction_r</coordinate>
                <optimal_force>5</optimal_force>
            </CoordinateActuator>
            <CoordinateActuator name="hip_rotation_r_reserve">
                <min_control>-Inf</min_control>
                <max_control>Inf</max_control>
                <coordinate>hip_rotation_r</coordinate>
                <optimal_force>1</optimal_force>
            </CoordinateActuator>
            <CoordinateActuator name="knee_angle_r_reserve">
                <min_control>-Inf</min_control>
                <max_control>Inf</max_control>
                <coordinate>knee_angle_r</coordinate>
                <optimal_force>1</optimal_force>
            </CoordinateActuator>
            <CoordinateActuator name="ankle_angle_r_reserve">
                <min_control>-Inf</min_control>
                <max_control>Inf</max_control>
                <coordinate>ankle_angle_r</coordinate>
                <optimal_force>1</optimal_force>
            </CoordinateActuator>
            <CoordinateActuator name="hip_flexion_l_reserve">
                <min_control>-Inf</min_control>
                <max_control>Inf</max_control>
                <coordinate>hip_flexion_l</coordinate>
                <optimal_force>2.5</optimal_force>
            </CoordinateActuator>
            <CoordinateActuator name="hip_adduction_l_reserve">
                <min_control>-Inf</min_control>
                <max_control>Inf</max_control>
                <coordinate>hip_adduction_l</coordinate>
                <optimal_force>5</optimal_force>
            </CoordinateActuator>
            <CoordinateActuator name="hip_rotation_l_reserve">
                <min_control>-Inf</min_control>
                <max_control>Inf</max_control>
                <coordinate>hip_rotation_l</coordinate>
                <optimal_force>1</optimal_force>
            </CoordinateActuator>
            <CoordinateActuator name="knee_angle_l_reserve">
                <min_control>-Inf</min_control>
                <max_control>Inf</max_control>
                <coordinate>knee_angle_l</coordinate>
                <optimal_force>1</optimal_force>
            </CoordinateActuator>
            <CoordinateActuator name="ankle_angle_l_reserve">
                <min_control>-Inf</min_control>
                <max_control>Inf</max_control>
                <coordinate>ankle_angle_l</coordinate>
                <optimal_force>1</optimal_force>
            </CoordinateActuator>
            <CoordinateActuator name="mtp_angle_r_reserve">
```

```
                <min_control>-Inf</min_control>
                <max_control>Inf</max_control>
                <coordinate>mtp_angle_r</coordinate>
                <optimal_force>1</optimal_force>
            </CoordinateActuator>
            <CoordinateActuator name="mtp_angle_l_reserve">
                <min_control>-Inf</min_control>
                <max_control>Inf</max_control>
                <coordinate>mtp_angle_l</coordinate>
                <optimal_force>1</optimal_force>
            </CoordinateActuator>
            <CoordinateActuator name="subtalar_angle_r_reserve">
                <min_control>-Inf</min_control>
                <max_control>Inf</max_control>
                <coordinate>subtalar_angle_r</coordinate>
                <optimal_force>1</optimal_force>
            </CoordinateActuator>
            <CoordinateActuator name="subtalar_angle_l_reserve">
                <min_control>-Inf</min_control>
                <max_control>Inf</max_control>
                <coordinate>subtalar_angle_l</coordinate>
                <optimal_force>1</optimal_force>
            </CoordinateActuator>
            <CoordinateActuator name="knee_angle_r_beta_reserve">
                <min_control>-Inf</min_control>
                <max_control>Inf</max_control>
                <coordinate>knee_angle_r_beta</coordinate>
                <optimal_force>1</optimal_force>
            </CoordinateActuator>
            <CoordinateActuator name="knee_angle_l_beta_reserve">
                <min_control>-Inf</min_control>
                <max_control>Inf</max_control>
                <coordinate>knee_angle_l_beta</coordinate>
                <optimal_force>1</optimal_force>
            </CoordinateActuator>
            <CoordinateActuator name="med_cond_adduction_r_reserve">
                <min_control>-Inf</min_control>
                <max_control>Inf</max_control>
                <coordinate>med_cond_adduction_r</coordinate>
                <optimal_force>1</optimal_force>
            </CoordinateActuator>
            <CoordinateActuator name="med_cond_adduction_l_reserve">
                <min_control>-Inf</min_control>
                <max_control>Inf</max_control>
                <coordinate>med_cond_adduction_l</coordinate>
                <optimal_force>1</optimal_force>
            </CoordinateActuator>
            <CoordinateActuator name="lat_cond_adduction_r_reserve">
                <min_control>-Inf</min_control>
                <max_control>Inf</max_control>
                <coordinate>lat_cond_adduction_r</coordinate>
                <optimal_force>1</optimal_force>
            </CoordinateActuator>
            <CoordinateActuator name="lat_cond_adduction_l_reserve">
                <min_control>-Inf</min_control>
                <max_control>Inf</max_control>
                <coordinate>lat_cond_adduction_l</coordinate>
                <optimal_force>1</optimal_force>
            </CoordinateActuator>
% ------------------------------------------------------------
        </objects>
    </ForceSet>
</OpenSimDocument>
```

G

Reserve actuator and other muscle activations

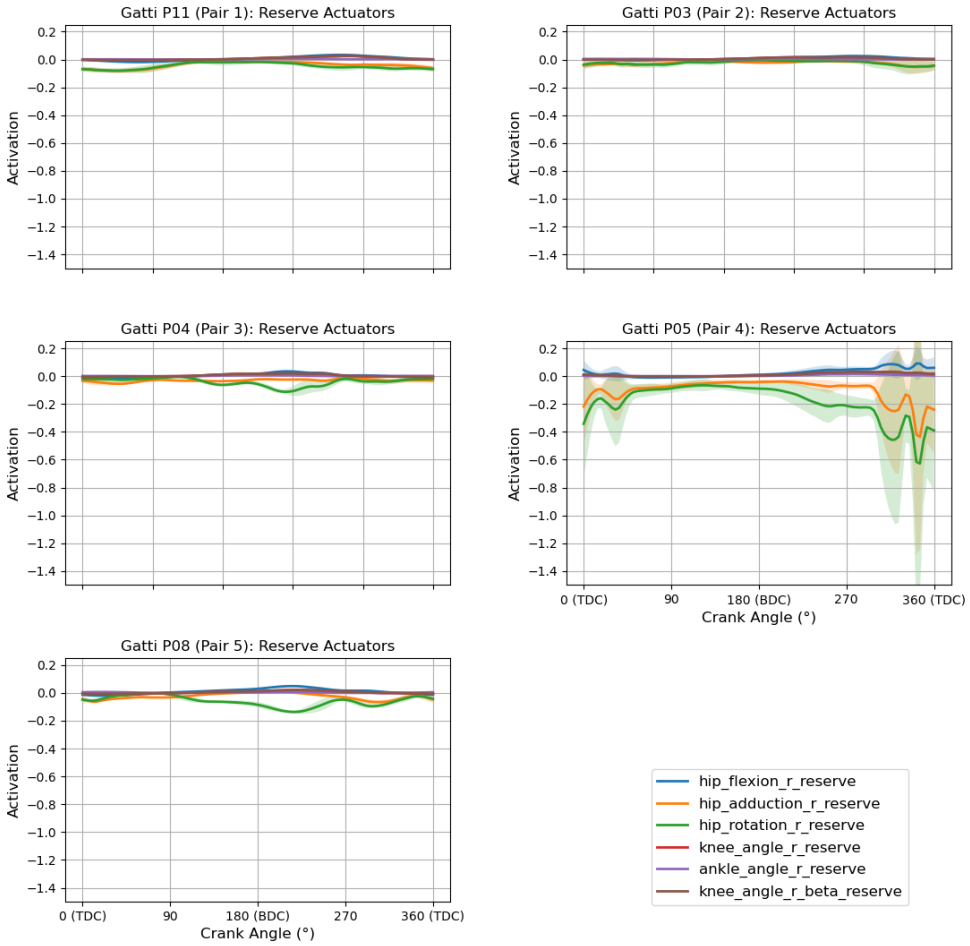

Figure G.1: Mean ± 1SD of the reserve actuator activations for ten consecutive crank cycles. For subject Gatti P05, increased reserve actuator activations are observed, particularly during the upstroke phase. Subject P11, P03, P04, P08 reserve actuators show low and stable activations.

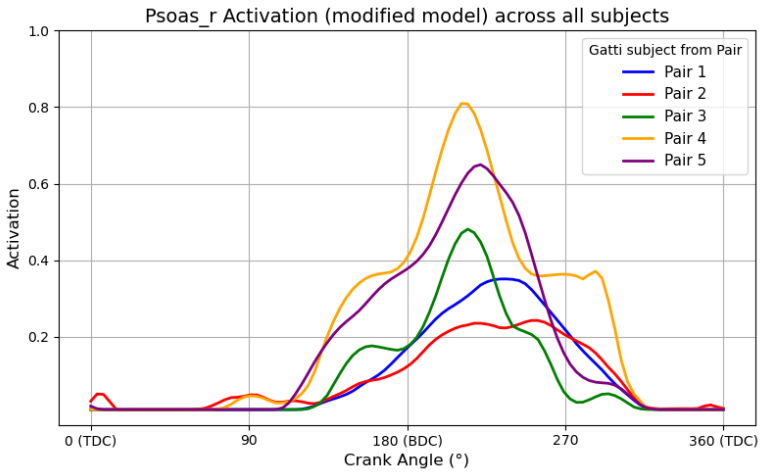

Figure G.2: Model-predicted Iliopsoas activation across five participants from the online dataset. High activations are observed in multiple cases, especially during the upstroke phase.

H

Pedal reaction force estimation

This appendix outlines a detailed description on the methods used to try to estimate the Pedal Reaction Forces (PRF). These forces represent the PRF that we could not measure due to broken sensors during the experiments (Appendix D). A detailed description of the estimation process is provided for transparency and reproducibility purposes.

H.1. Available data and constraints

- Marker-based motion capture (joint angles, marker positions)
- Average Cadence and Power Output
- Mesh file of crank body
- Mesh file of bike frame body

H.1.1. Adding crank + bike frame

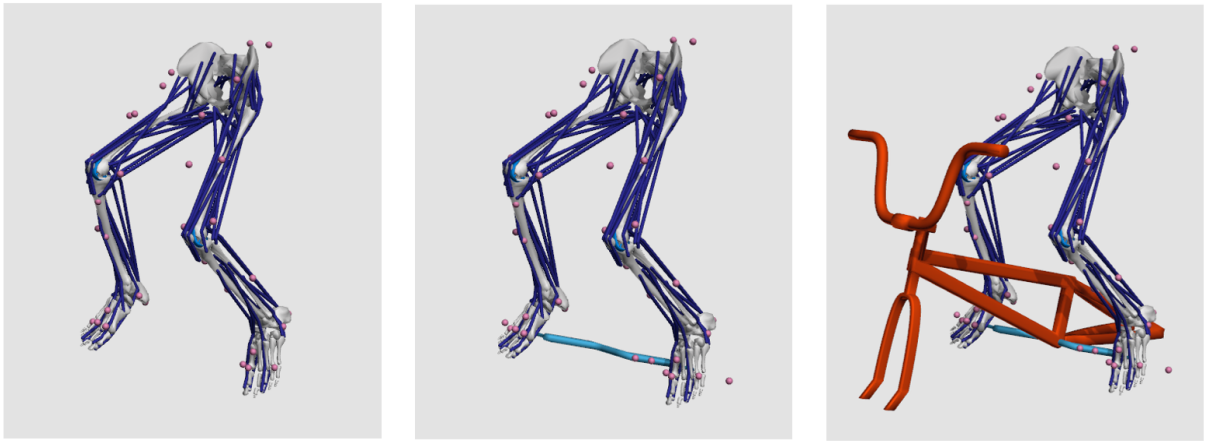

Figure H.1: Incorporation of the crank and frame bodies into the OpenSim musculoskeletal model. From left to right: Static cycling position model, Static cycling position with feet constrained to crank body, Static cycling body with feet constraint to crank body and crank body attached to frame body, which is locked with respect to the ground.

H.1.2. PointOnLineConstraints between the feet and the pedals

The following PointOnLine constraints were added to the ConstraintsSet of the modified musculoskeletal model.

Listing H.1: PointOnLineConstraint setup for the left and the right foot-pedal interaction

```
<PointOnLineConstraint name="constraintR">
    <!--Path to a Component that satisfies the Socket 'line_body' of type PhysicalFrame.-->
    <socket_line_body>/bodyset/bracket</socket_line_body>
    <!--Path to a Component that satisfies the Socket 'follower_body' of type PhysicalFrame.-->
    <socket_follower_body>/bodyset/toes_r</socket_follower_body>
    <!--Direction of the line specified in the line body frame.-->
    <line_direction_vec>0 0 1</line_direction_vec>
    <!--The default point on the line specified in the line body frame.-->
    <point_on_line>0 0.14999999999999999 -0.17249999999999999</point_on_line>
    <!--The point on (and specified in) the follower body constrained to the line.-->
    <point_on_follower>-0.050000000000000003 0 0</point_on_follower>
</PointOnLineConstraint>

<PointOnLineConstraint name="constraintL">
    <!--Path to a Component that satisfies the Socket 'line_body' of type PhysicalFrame.-->
    <socket_line_body>/bodyset/bracket</socket_line_body>
    <!--Path to a Component that satisfies the Socket 'follower_body' of type PhysicalFrame.-->
    <socket_follower_body>/bodyset/toes_l</socket_follower_body>
    <!--Direction of the line specified in the line body frame.-->
    <line_direction_vec>0 0 1</line_direction_vec>
    <!--The default point on the line specified in the line body frame.-->
    <point_on_line>0 -0.157 0.17249999999999999</point_on_line>
    <!--The point on (and specified in) the follower body constrained to the line.-->
    <point_on_follower>-0.050000000000000003 0 0</point_on_follower>
</PointOnLineConstraint>
```

H.1.3. Topology overview

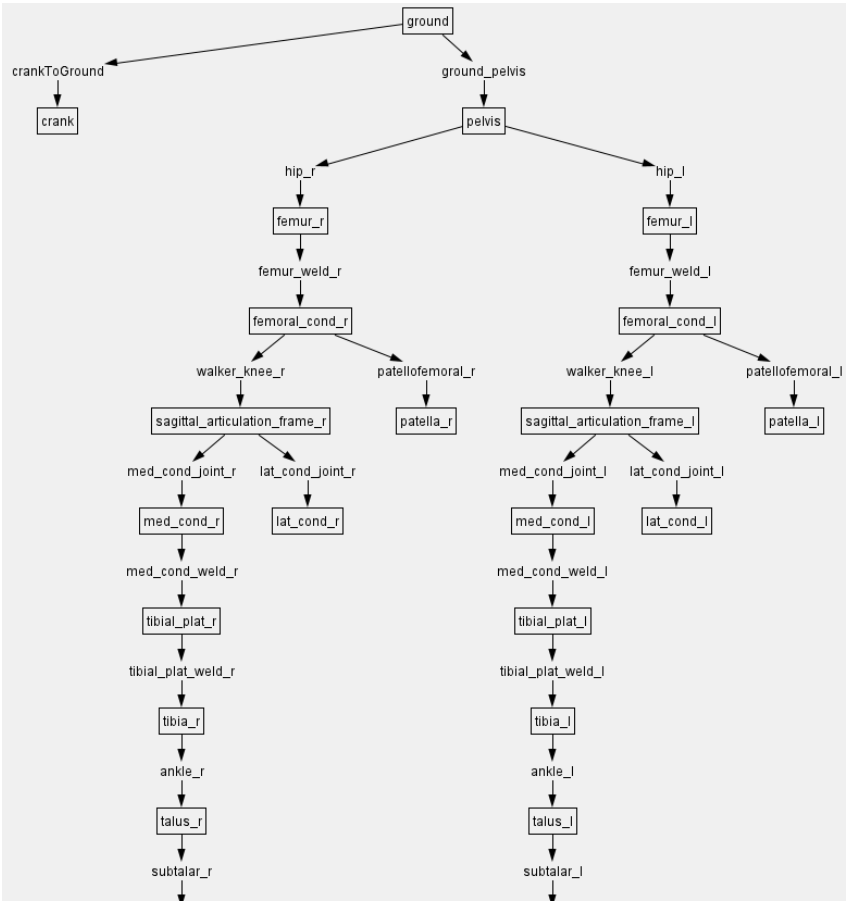

(a) Topology with crank and joint

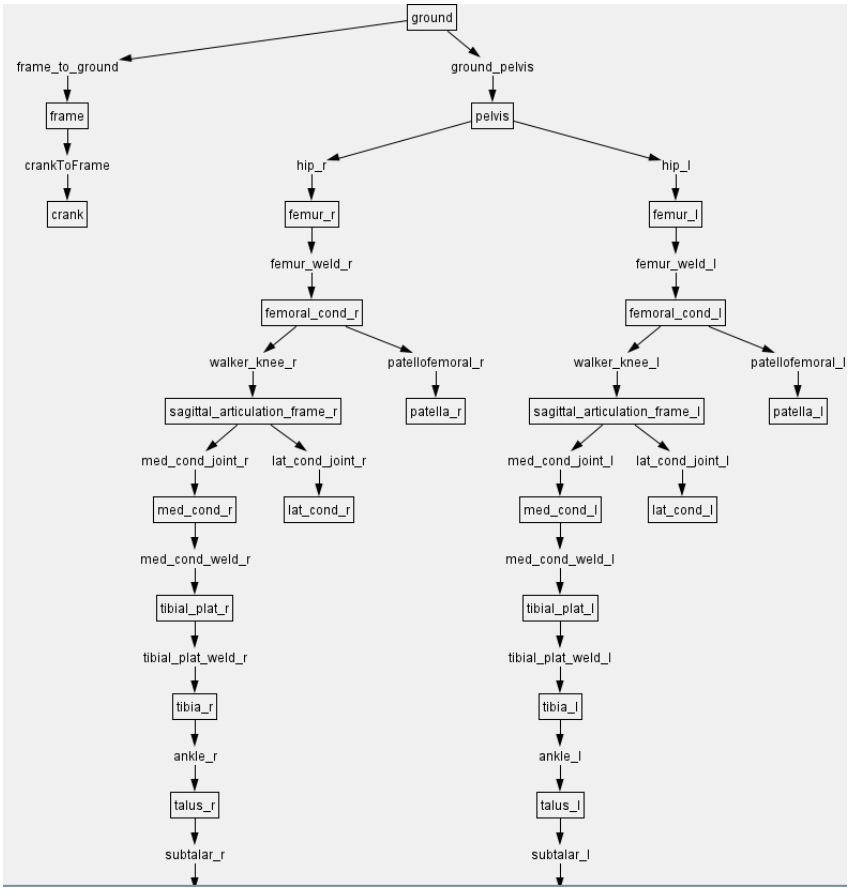

(b) Topology with bike frame body, crank and joints

Figure H.2: Comparison of topologies

H.2. Attempted approaches

H.2.1. Static optimisation

A crank body and a frame body were added to the musculoskeletal model (Figure H.2). The objective was to get static optimisation (SO) running with the two PointOnLine constraints between the feet and the pedals enforced (Listing H.1). During the application of SO in OpenSim, two recurring errors were observed:

1. Muscle activations reached or approached their maximum of 1, indicating that the muscles were not strong enough to produce the required joint torques.
2. Acceleration-level constraint violations occurred in constrained coordinates.

The first issue is straightforward to resolve by increasing the maximal isometric force of the muscles. This would allow the optimisation problem to converge, though at the cost of physiological realism. The second issue, however, is more fundamental.

SO attempts to minimize muscle activation while tracking both marker positions and coordinate accelerations. These accelerations are computed as the second derivative of the marker trajectories obtained from Inverse Kinematics (IK). When no constraints are active in the model, this generally works well. In that case, the solver is able to track both markers and accelerations rather well (normal constraint violation = $\pm 10e^{-13}$).

However, once the PointOnLine constraints are introduced, the optimisation problem becomes overconstrained. The solver is now pulled in three directions: matching marker trajectories, matching coordinate accelerations, and satisfying constraints.

The root of the problem lies in how accelerations are derived. Because SO calculates coordinate accelerations by differentiating marker positions, any minor error in the marker trajectories gets amplified. This is particularly problematic for coordinates involved in the constraints (such as `ankle_angle_r` and `ankle_angle_l`), where even small mismatches in marker data lead to large discrepancies in the estimated accelerations.

Even though constraints are defined in the model, SO does not strictly enforce them. That is, it does not solve them as hard equality constraints within the optimisation process. Instead, it operates under the assumption that the kinematics already satisfy the constraints reasonably well, and continues with its optimisation. In practice, this means that SO seems to try to respect the constraints, but lacks the mechanism to actively enforce them. This leads to instability when the constraints, marker data, and computed accelerations are even slightly inconsistent. This is likely what caused the optimisation to fail at each time frame.

Reducing the assembly tolerance (e.g. from 10^{-5} to 10^{-3}) was tested in an attempt to alleviate the issue, but this did not prevent SO from failing.

H.2.2. Computed Muscle Control

Computed Muscle Control (CMC) was used as an alternative to SO. Unlike SO, CMC does attempt to actively satisfy kinematic constraints during the simulation. Additionally, CMC is more robust to inconsistencies in the Inverse Kinematics (IK) solution that often cause SO to fail.

Different from SO, which operates on a frame-by-frame basis, CMC performs a forward simulation that generates a continuous, muscle-driven motion. It accounts for muscle activation dynamics and tendon compliance, which makes it more physiologically accurate, but also more complex and computationally expensive.

An important benefit of CMC is the `<use_fast_optimisation_target>` option, which was set to `false` in this case. This setting allowed the solver to approximate desired accelerations rather than strictly enforcing them, providing greater robustness in constrained models.

Despite these advantages, CMC also failed to produce a stable solution. The solver also struggled to simultaneously track the desired kinematics, respect the constraints, and enforce realistic muscle activation dynamics. This is likely due to the model being overconstrained and the experiments being conducted inconsistently (different bike/saddle/handlebar locations).

To illustrate this, the pelvic translations were plotted for three different motion files, see Figure H.6, H.7 and H.8.

The figure shows large differences in pelvis translations across three cases:

1. IK solution without any crank or PointOnLine constraints (IK solution as used in the rest of the study).
2. IK solution with the crank body and the two PointOnLine constraints enforced.
3. CMC solution with the crank body and the two PointOnLine constraints enforced.

These deviations highlight how the body is forced to compensate for inconsistencies between the kinematics, constraints, and muscle dynamics.

- **Figure H.3 (Pelvis Tilt)**: The blue IK solution remains the most consistent and physiologically reasonable across the full cycle. It shows regular oscillations with a clear and stable amplitude. The orange (IK with crank and constraints) and green (CMC with constraints) solutions follow a broadly similar waveform but have a reduced amplitude and tend to lean more backwards.

  These differences suggest that the added constraints restrict natural pelvis tilt and introduce coordination errors not present in the reference model.
- **Figure H.4 (Pelvis List)**: Pelvis list should oscillate around zero during cycling to reflect balanced lateral motion. The blue IK solution does this correctly. The orange and green lines show a strong positive bias, with the pelvis consistently hanging to the right. This is likely due to scaling errors or joint placement mismatches—making it harder for the model to reach the right pedal. As a result, the pelvis tilts further to compensate, and the constraints force it into this offset. It's not physiological, and it refers to problems with how the constraints are set up.
- **Figure H.5 (Pelvis Rotation)**: The constrained IK solution exaggerates the movement slightly, while the CMC trace swings more widely and erratically.
- **Figure H.6 (Vertical Translation, pelvis_ty)**: The vertical position of the pelvis should remain stable. The IK solutions achieves this. The CMC solution shows exaggerated vertical motion. This suggests that the pelvis-saddle interaction is not being enforced properly in forward dynamics. Constraints are either too loose or ineffective.
- **Figure H.7 (Medial-Lateral Translation, pelvis_tx)**: The blue IK model holds the pelvis close to the midline, as it should, because the bike was place at 0 w.r.t. the ground frame. The orange solution introduces minor drift. The green CMC trace shows wide side-to-side swings that are not realistic.
- **Figure H.8 (Anterior-Posterior Translation, pelvis_tz)**: The IK outputs maintains a steady position, as expected for anterior-posterior movement during seated cycling. The constrained IK solution does show an unnatural double-peak pattern.

These comparisons illustrate that while CMC roughly follows the motion derived from IK, it adds substantial movement in directions that are otherwise constrained or suppressed in the IK solutions. This behavior confirms that CMC introduces more natural but less restricted dynamics, which can become problematic if the model lacks proper constraint definition or mechanical grounding.

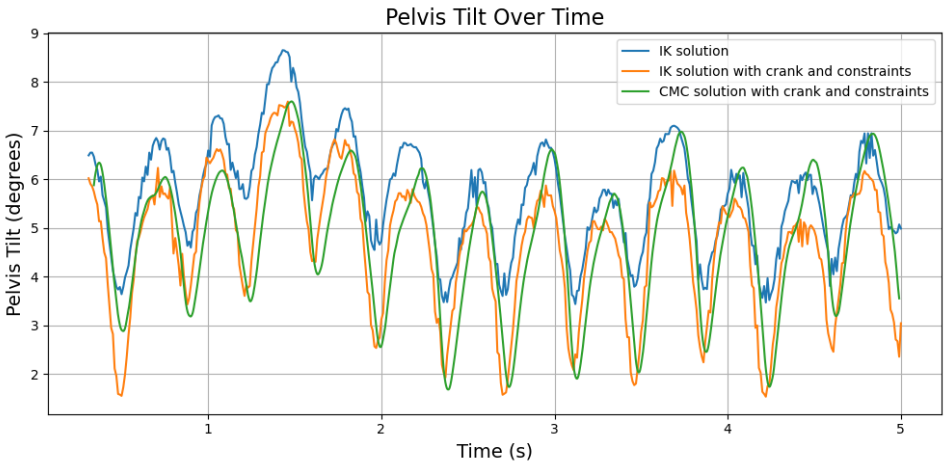

Figure H.3: Comparison of pelvis tilt over time between IK and CMC solutions.

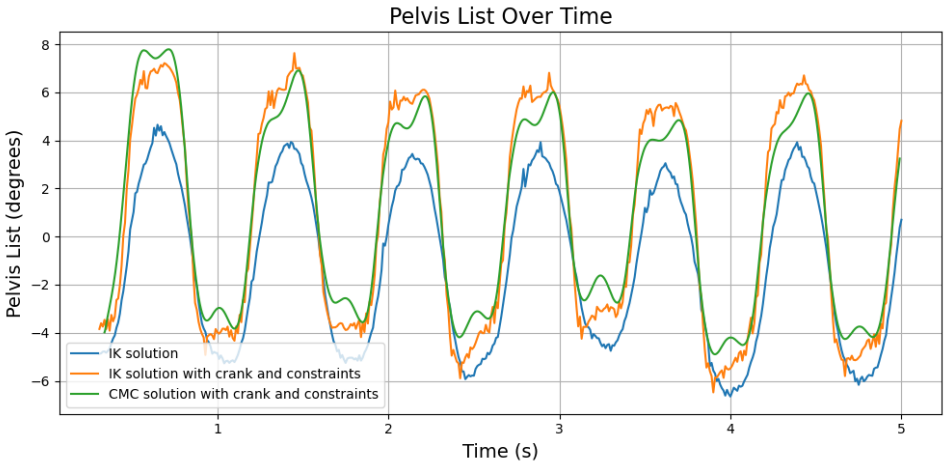

Figure H.4: Comparison of pelvis list over time between IK and CMC solutions.

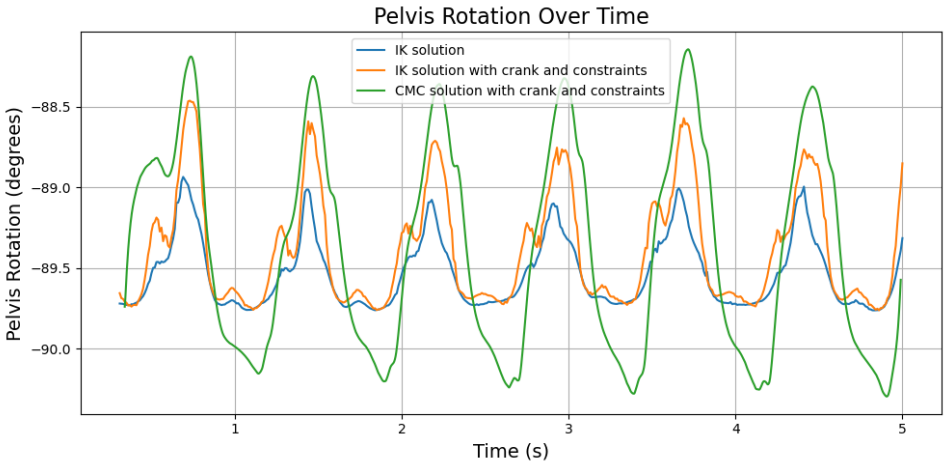

Figure H.5: Comparison of pelvis rotation over time between IK and CMC solutions.

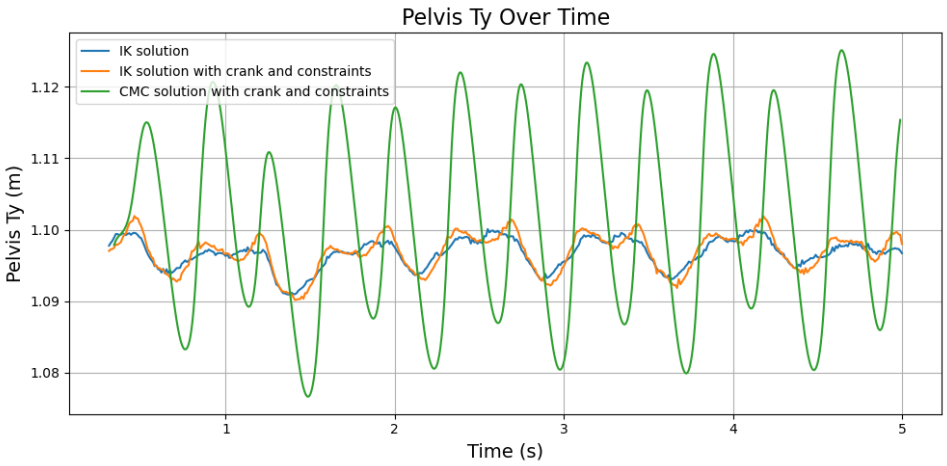

Figure H.6: Comparison of vertical pelvis translation (pelvis_ty) over time between IK and CMC solutions.

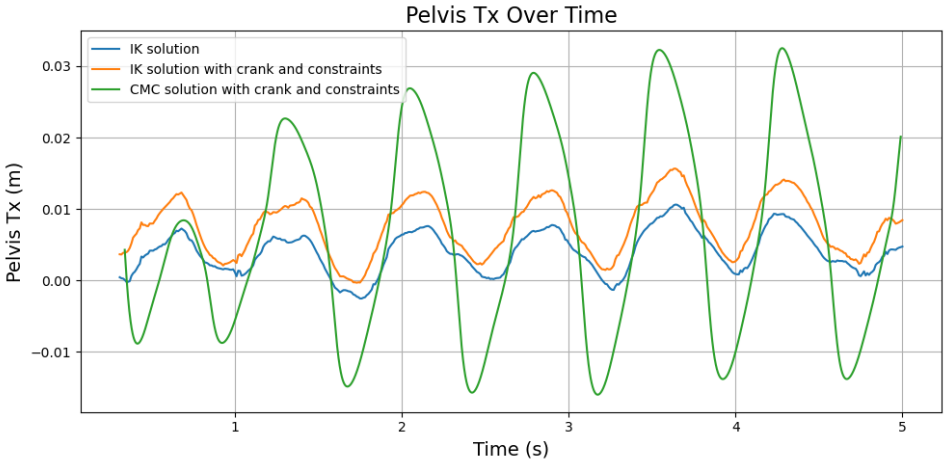

Figure H.7: Comparison of medial-lateral pelvis translation (pelvis_tx) over time between IK and CMC solutions.

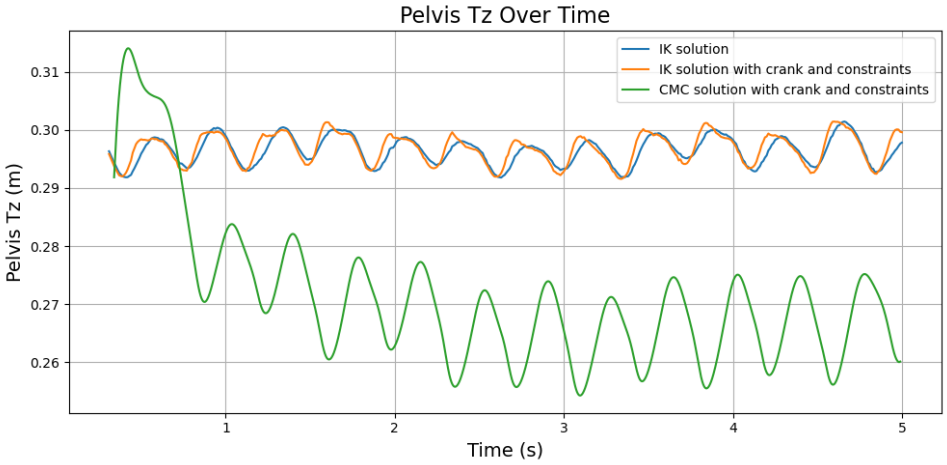

Figure H.8: Comparison of anterior-posterior pelvis translation (pelvis_tz) over time between IK and CMC solutions.

Incorporation of external torque

To address the instability and solver failures, we explored adding an external torque to the crank. Initially, we assumed this would not be necessary, since the crank is constrained and we hypothesized that

the model should be able to simulate the motion without an explicit torque input. However, adding an external torque becomes more intuitive when considering the nature of the crank setup. Without an actual reaction force from the pedal, the legs are effectively floating during the downward phase of the motion. The model compensates by generating large co-contractions to create artificial stability, resulting in unrealistic muscle forces and control instability. With Computed Muscle Control (CMC), a torque representing the resistance of the system can be added, which results in a reaction force at the foot-pedal joint. These reaction forces represent the missing pedal reaction forces. We could estimate the torque with the average power output (Equation H.1).

$$\tau = \frac{P}{\omega} = \frac{100}{8.38} \approx 11.93\,\text{Nm} \tag{H.1}$$

External torque file

As a first approach, we used the `ExternalForce` object to apply torque data from a `.mot` file. This file was linked through an XML configuration and referenced in the CMC tool via the external loads setting (Listing H.2).

Listing H.2: External torque setup using ExternalForce

```
<?xml version="1.0" encoding="UTF-8"?>
<OpenSimDocument Version="30000">
  <InverseDynamicsTool name="both_pedal_forces">
    <objects>
      <ExternalForce name="crank">
        <torque_identifier>right_torque_</torque_identifier>
        <data_source_name>pedal_torque.mot</data_source_name>
      </ExternalForce>
    </objects>
    <groups/>
    <datafile>pedal_torque.mot</datafile>
    <external_loads_model_kinematics_file/>
    <lowpass_cutoff_frequency_for_load_kinematics>6</
        lowpass_cutoff_frequency_for_load_kinematics>
  </InverseDynamicsTool>
</OpenSimDocument>
```

The torque data in this file was based on an average estimate derived from cycling power. Despite this straightforward setup, no visible effect was observed in either Inverse Dynamics or CMC.

Prescribed force addition to the model

Next, we tried a more direct method using the `PrescribedForce` object in the OpenSim model (Listing H.3). This should, in theory, always be enforced during the simulation. A constant torque of $-11.93\,\text{Nm}$ (Equation H.1) was applied to the crank in the z-direction. This torque was applied consistently over time and was not tied to a time-varying signal. The expected result was improved stability in the model and more realistic muscle behavior. Unfortunately, the torque had no measurable effect in either ID or CMC.

Listing H.3: PrescribedForce setup for crank torque

```
<PrescribedForce name="crank_torque">
  <applied_to_body>crank</applied_to_body>
  <point>0 0 0</point>
  <force_expressed_in_body>crank</force_expressed_in_body>
  <point_expressed_in_body>crank</point_expressed_in_body>

  <force_functions>
    <Constant name="fx"><value>0</value></Constant>
    <Constant name="fy"><value>0</value></Constant>
    <Constant name="fz"><value>0</value></Constant>
  </force_functions>

  <torque_functions>
    <Constant name="tx"><value>0</value></Constant>
    <Constant name="ty"><value>0</value></Constant>
    <Constant name="tz"><value>-11.93</value></Constant>
  </torque_functions>
</PrescribedForce>
```

A possible explanation is that the crank is not mechanically connected to the feet via joints, but in this setup only through constraints. In OpenSim, constraints might not create a valid force transmission path like joints do. As a result, the torque cannot propagate up the kinetic chain to affect the foot or knee. For this to work, a physical connection would be needed (e.g., a pin or weld joint), but adding such a joint would introduce a closed kinematic loop. This is something OpenSim does not support and would require a fundamental restructuring of the model.

Furthermore, a welded connection would also be physically unrealistic, as the foot naturally moves relative to the pedal during cycling.

Additionally, another limitation is that using only kinematics to estimate the PRF gives the minimum kinetics needed to produce the motion, without capturing shear forces or other losses during propulsion. This can give a misleading picture of how forces act on the knee joint. Because of these issues, this method is unlikely to be useful for further analysis.

In conclusion, although adding an external or prescribed torque seemed like the most direct and logical fix, neither method solved the instability. The problem appears to lie in the mismatch between the model's structure and its ability to transfer external torques to the legs. Fixing this would require restructuring the models topology entirely.

H.3. Recommendations

If, for any reason, PRF need to be estimated through musculoskeletal modelling rather than measured directly, the following steps are recommended.

Naturally, using instrumented pedals capable of measuring 6-DOF forces remains the most reliable and accurate method for capturing PRFs. However, when such equipment is unavailable, a simulation-based approach can be applied, similar to how it is tried in this study, but with the following considerations:

1. **Use CMC.** Rather than SO, CMC better handles dynamic constraints and muscle activation dynamics. CMC offers more stability and realism in muscle-driven simulations, especially when constraints are involved.
2. **Reconsider the connection between feet and pedals.** In order for external torques or reaction forces to propagate through the kinetic chain, the feet might need to be mechanically connected to the pedals using a joint (e.g., a pin joint). This requires rebuilding the model topology to avoid a closed-loop system and to maintain a valid kinematic chain.
3. **Improve motion capture setup.** Future experiments should include markers on the bike (frame, crank, and pedals) to accurately define the position and orientation of the bike in space. In addition, the height of the bike frame, as well as the vertical and horizontal position of the handlebar and the saddle, should be measured and documented accurately.
4. **Machine learning model approach.** Finally, recent research proved that Machine Learning models are able to predict PRF, using only the crank angle, cadence, power output, and participants' weight and height at each time frame as input [123].

These improvements are necessary to reconstruct the experimental setup and ensure valid simulation results. In this project, these data were unfortunately not captured, as the decision to estimate PRFs using musculoskeletal modelling was made at the last moment.

I

Kinematics

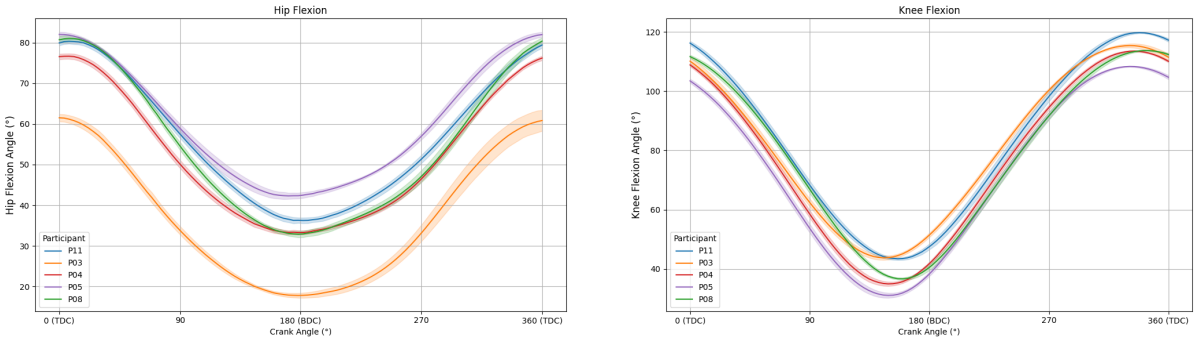

(a) Hip flexion angles (right leg)

(b) Knee flexion angles (right leg)

Figure I.1: Mean hip and knee flexion angles of the right leg over one crank cycle (0°–360°) for five participants, averaged across 10 crank cycles. Both joints show a cyclic flexion-extension pattern. Participant P03 stands out with distinctly lower hip flexion throughout the cycle, while knee flexion shows consistent trends but varying peak angles across individuals.

J

Kinetics

J.1. Joint moments

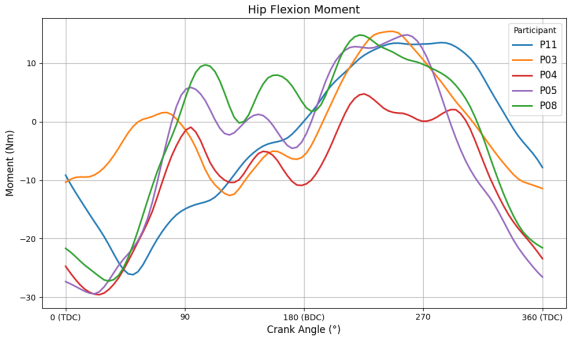

(a) Hip flexion moment. Flexion moment is positive.

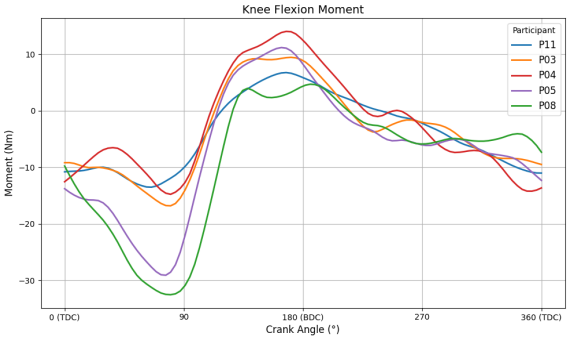

(b) Knee flexion moment. Flexion moment is positive.

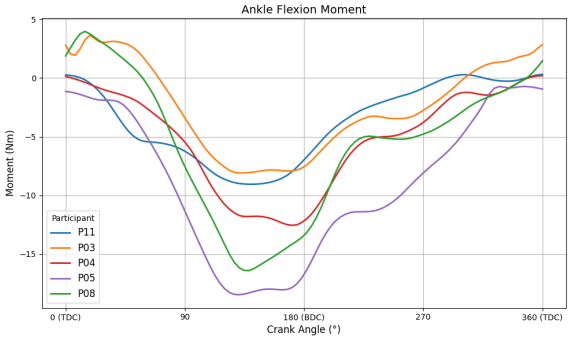

(c) Ankle flexion moment. Flexion moment is positive.

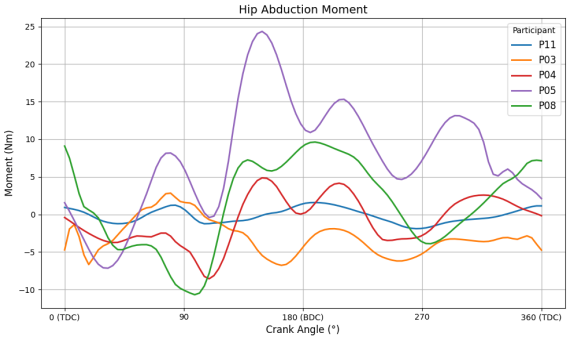

(d) Hip abduction moment. Abduction moment is positive (frontal plane).

Figure J.1: Joint moments (mean over 10 crank cycles) for five participants across one crank revolution (0°–360°). Data includes (a) hip flexion, (b) knee flexion, (c) ankle flexion, and (d) hip abduction moments. All moments were estimated using OpenSim inverse dynamics based on filtered kinematics (6 Hz) and pedal reaction force data.

J.2. Pedal reaction forces

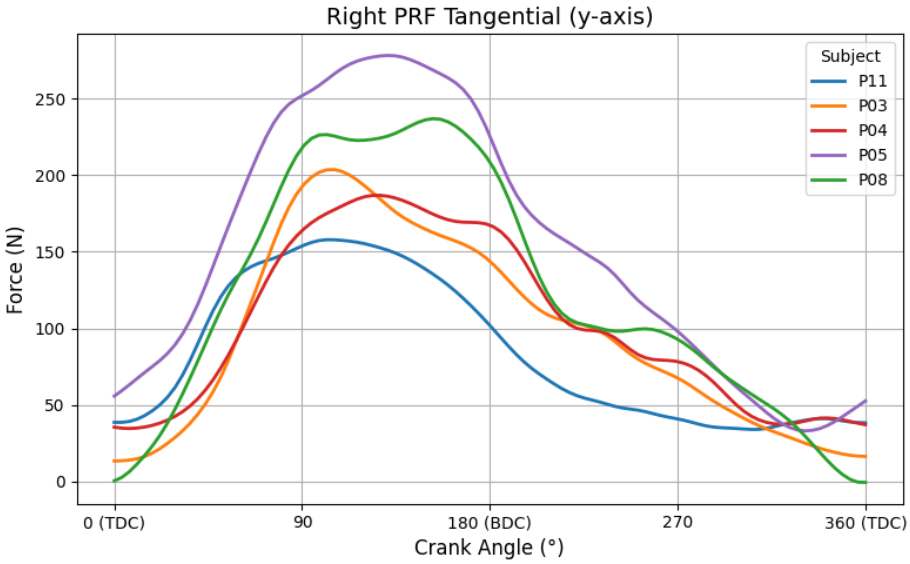

(a) Tangential PRF (Y direction): positive forces act in the direction of crank rotation, contributing to forward crank torque.

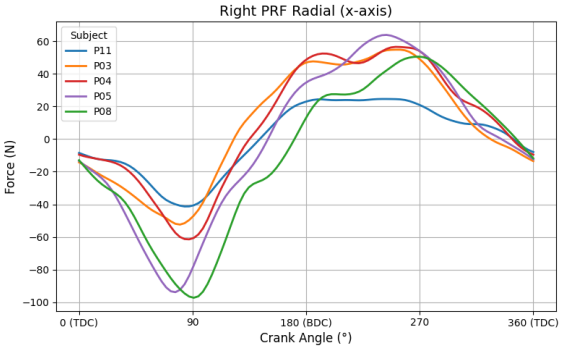

(b) Radial PRF (X direction): positive forces act outward along the crank arm, away from the crank axis; negative forces act inward.

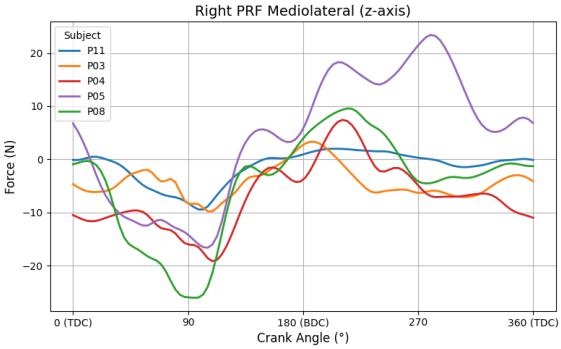

(c) Mediolateral PRF (Z direction): positive forces act laterally (away from the bike midline); negative forces act medially (toward the midline).

Figure J.2: Mean pedal reaction forces (PRF over one crank cycle (0°–360°) for five participants, averaged over 10 cycles. (a) Tangential forces dominate the contribution to crank torque and show the most pronounced inter-individual differences, primarily due to variations in power output and cadence. (b) Radial and (c) mediolateral forces provide insight into additional loading components that do not directly contribute to crank rotation but influence joint and muscle loading.

K

Comparison of OpenSim workflows

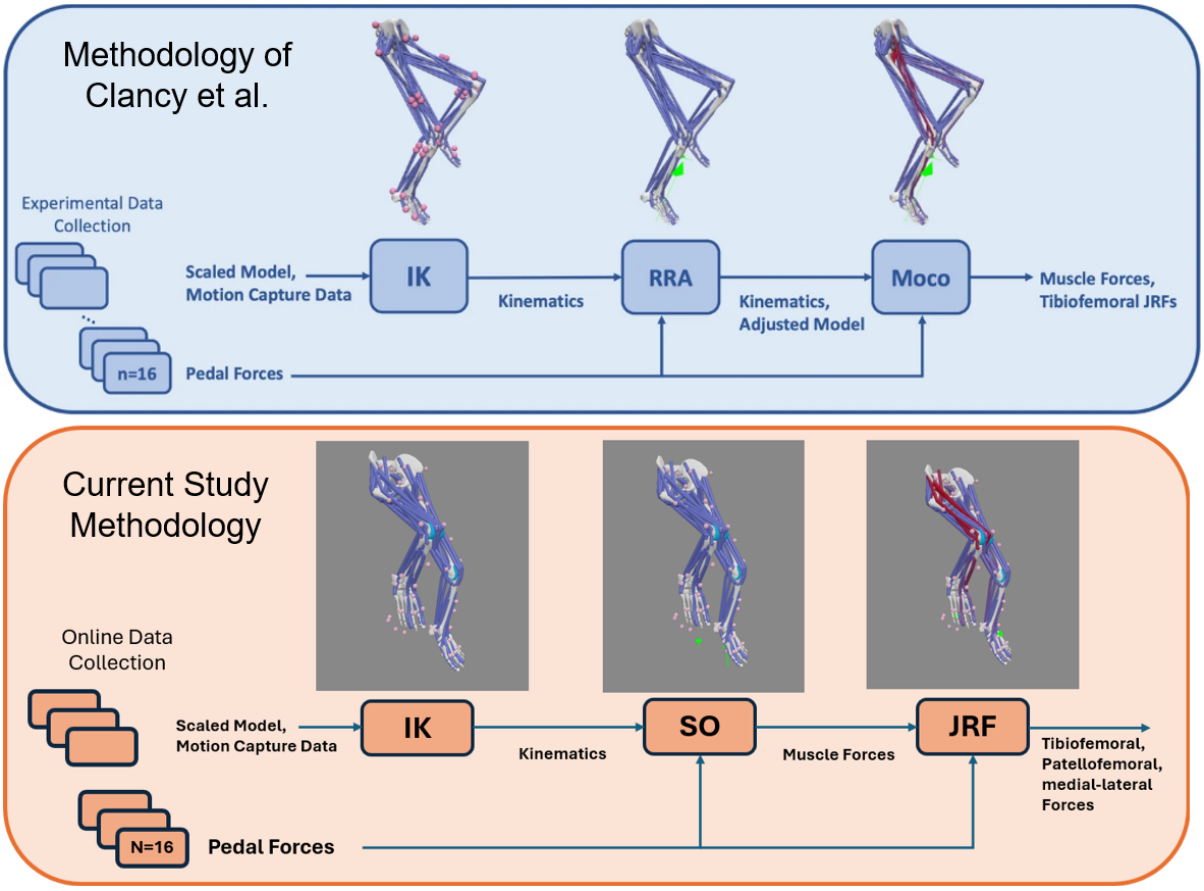

Figure K.1: Comparison of the OpenSim modelling workflows used by Clancy et al. and the current study. The original workflow employed a residual reduction algorithm (RRA) and motion optimisation (Moco) to refine kinematics and estimate joint reaction forces (JRF), while the current study uses a streamlined pipeline combining inverse kinematics (IK), static optimisation (SO), and direct JRF estimation. The adapted workflow enables compartment-specific force analysis while maintaining alignment with the original validation framework.